Journal of Molecular Liquids 398 (2024) 124213

Contents lists available at ScienceDirect

Journal of Molecular Liquids

journal homepage: www.elsevier.com/locate/molliq

Tuning adsorption capacities of hybrid mesoporous silica nanospheres and adsorption mechanism study for sulfamethoxazole and diclofenac removal from water

Josefa Ortiz-Bustos [a], Sofia F. Soares [b], Helena Pérez del Pulgar [a], Yolanda Pérez [a], Santiago Gómez-Ruiz [a], Ana Luísa Daniel-da-Silva [b,*], Isabel del Hierro [a,b,*]

[a] Grupo COMET-NANO, Departamento de Biología Geología, Física y Química Inorgánica, ESCET, Universidad Rey Juan Carlos, C/Tulipán S/N Móstoles, Madrid, Spain
[b] CICECO-Aveiro Institute of Materials, Department of Chemistry, University of Aveiro, Aveiro 3810-193, Portugal

ARTICLE INFO

Keywords:
Hybrid mesoporous silica
Adsorption
Diclofenac
Sulfamethoxazole

ABSTRACT

The functionalization of mesoporous silica nanospheres and mesoporous hybrid core–shell magnetic silica nanospheres has been carried out through post-synthetic procedures, and these materials have been tested as adsorbents for the removal of sulfamethoxazole (SMX) and diclofenac (DF) from water. The effects of the silica material and the types of functionalities anchored on the silica surface have been investigated. Additionally, the unreacted silanol groups on the silica surface have been capped with hydrophobic trimethylsilyl groups to modify the hydrophilic-hydrophobic properties of the materials. The materials have been characterized by textural, spectroscopic, and microscopic techniques. The maximum adsorption capacity and kinetics of adsorption were determined using adsorption and kinetic theoretical models. The experimental results indicate that both the surface area and the presence of specific functionalities on the silica surface, including zwitterionic groups like hydroxide choline and methyl p-toluene sulfonate choline, have a significant impact on the material's adsorption capacity. The adsorption studies revealed that the highest adsorption capacity (q_t) for DF (80.7 mg L^{-1}) and SMX (27.2 mg L^{-1}) was achieved with PTS-Chol-MSN, which consists of mesoporous silica nanospheres possessing a larger surface area, unprotected silanol groups and the methyl p-toluene sulfonate choline functionality on its surface. The mechanism of drug adsorption involves physical and chemical adsorptions with the presence of H-bonding and π-π stacking interactions.

1. Introduction

The presence of emergent pollutants (EPs), compounds such as hormones, antibiotics, pesticides, and others, many of which are listed as endocrine-disrupting chemicals, has significantly increased in the past decade [1]. In certain cases, the release of these emerging pollutants into the environment may have been ongoing for some time; however, their recognition has been delayed until more precise detection methods have been established [2,3]. Currently, EPs are not included in routine monitoring programs and their behavior and ecotoxicological effects, are often not well understood.

The removal of these contaminants through common treatments poses a challenge due to their low concentrations in the environment and raw water, making it difficult to eliminate them using standard water treatment methods. Besides, the development of advanced drinking water treatments specifically targeting these EPs often requires significant energy and chemical consumption. Among the most used and efficient water treatment processes at pilot or full scale are membrane-based processes (micro, ultra, and nanofiltration, reverse and forward osmosis, membrane bioreactors, and electrodialysis), advanced oxidation processes (chemical, electro-chemical, ultrasounds processes, and photochemical processes) and adsorption processes. Often, a combination of these methods is employed [4].

Adsorption is an efficient and cost-effective process for the removal of EPs, provided that the adsorbent is economically accessible and possesses suitable characteristics such as high surface area and porosity. Additionally, the adsorbent should be easy to handle and capable of thermal or chemical regeneration. Commonly used adsorbents include activated carbon and carbonaceous materials [5], waste compounds from industries [6] agricultural by-products [7], and clays [8].

* Corresponding authors.
E-mail address: isabel.hierro@urjc.es (I. del Hierro).

https://doi.org/10.1016/j.molliq.2024.124213
Received 6 October 2023; Received in revised form 16 January 2024; Accepted 4 February 2024
Available online 9 February 2024

To increase EPs' removal efficiencies more specific organic, inorganic, or hybrid materials have been developed to obtain nano adsorbents with particle sizes in the range of 1–100 nm. These materials with improved adsorption properties can remove efficiently metals or organic compounds with different sizes and different chemical properties. Although nanomaterials can be used as adsorbents themselves their higher selectivity towards pollutants and higher price turn these materials into the perfect candidates to be incorporated into conventional membranes [9] or to support photo and electrocatalysts in water treatment processes [10 11]. Many different nanoscale materials have found applications for the removal of emerging micropollutants and pathogens from water, such as zeolites [12], metal oxides [13], noble metal nanoparticles [14], carbon nanotubes and fibers [15], graphene-based composites [16], etc.

Mesoporous silica materials have been widely recognized as excellent adsorbents for both organic and inorganic contaminants. Numerous studies have demonstrated that mesoporous silicas possess favorable characteristics for trapping contaminants from aqueous solutions, including high accessibility, cost-effectiveness, reusability, and exceptional ion exchange/adsorption capabilities [17]. One such silica-based material is MCM-41, which exhibits a large surface area, flexible pore structure, high pore volume, and non-toxicity, making it an ideal adsorbent candidate. The nanoscale pore channels within MCM-41 provide adsorption micro-interfaces that enhance energy and material transfer processes at the interface, leading to increased concentration and accumulation of pollutants and promoting reaction activation and advancement. More recently, magnetic mesoporous silica nanoparticles (MMSN) have been developed for the removal and magnetic separation of pollutants from contaminated water. These nanoparticles combine the enhanced adsorptive properties of mesoporous silica with the magnetic characteristics of iron oxide nanoparticles. Additionally, silica can be modified with organic molecules, enabling tuning of the hydrophobicity/hydrophilicity of the material's surface. This modification enhances the selectivity and adsorption of silica-based adsorbents [18].

The literature extensively reports the use of ionic liquids (ILs) for the removal of dyes, metal ions, organics, and various other pollutants from domestic and industrial sources [19,20]. Incorporating ILs into the pore structure of solid matrices is crucial for the development of supported ILs, which can overcome major drawbacks related to bulk ILs, including high viscosity, slow gas diffusivity, and high cost. Simultaneously, immobilizing "soft" ILs on the surface of "hard" solids can further modify and enhance the properties of the supports, such as wettability, lubricating properties, and separation efficiency. This approach allows the creation of tailored materials with improved performance for pollutant removal applications [21].

Immobilizing ILs onto porous matrices through covalent anchoring is an attractive strategy that helps prevent ILs from leaching, thereby minimizing the amount of IL required. Although the diversity of cations and anions in ILs is huge, the most widely known ILs are derived from rather expensive cations such as imidazolium, pyridinium, pyrrolidinium, and piperidinium. This limitation hinders their commercial-scale utilization. Additionally, some ILs are known for their toxicity and potential environmental impact, which further pose challenges to their widespread use.

With these precedents in mind, we have successfully incorporated a choline-based ionic liquid into the pores of mesoporous and magnetic mesoporous silica nanoparticles through covalent anchoring. Choline which is an affordable, biodegradable, and water-soluble organic salt has been chosen for its advantageous properties. It can be obtained from natural resources and is commonly classified within the B-complex vitamins.

In this study, we have investigated two different functionalities of choline-based ILs. Firstly, choline hydroxide, which comprises a quaternary ammonium salt, a hydroxyl group, and a hydroxide anion, was examined. The hydroxide can be easily substituted via an acid-base reaction with methyl p-toluene sulfonic acid, yielding choline methyl p-toluene sulfonate as the second functionality under investigation [22]. The synthesized materials have been characterized by the appropriate techniques. Subsequently, they were subjected to uptake studies involving the removal of sulfamethoxazole and diclofenac from water. These two pharmaceutical compounds widely used are found in wastewater at concentrations ranging from range μg/L to ng/L. Batch adsorption experiments and solid-state voltammetry techniques were employed to investigate the adsorption capacity and mechanisms. The aim was to understand how the functionalization process, characteristics of the silica material, and hydrophobic/hydrophilic surface properties influence the adsorption process. By conducting these investigations, we aimed to gain insights into the adsorption behavior, capacities, and mechanisms of the materials, particularly concerning the targeted pharmaceuticals, sulfamethoxazole, and diclofenac.

2. Experimental section

2.1. Materials

Tetraethylorthosilicate (TEOS) 98 %, 3-glycidyloxypropyltrimethoxysilane, trimethylamine solution 4.2 M in ethanol, tetramethylammonium hydroxide, methyl p-toluene sulfonic acid, sodium diclofenac, and sulfamethoxazole were purchased from Sigma Aldrich and used as received. Hexadecyltrimethylammonium bromide (CTAB), $FeCl_3{\cdot}6H_2O$, and $FeSO_4{\cdot}7H_2O$ were purchased from Acros and used as received. Toluene was purchased from Aldrich, respectively, distilled, and dried with appropriate drying agents before being used. Ethanol (synthesis quality) was purchased from SDS and used as received. Milli-Q water was used in the experiments.

2.2. Preparation of hybrid mesoporous silica nanospheres

The synthesis of the core–shell mesoporous silica nanospheres and the ionic-liquid surface functionalization were accomplished by using previously described methods [23,24], which are summarized in supplementary information.

2.3. Adsorption experiments

Before starting the experiment, stock sulfamethoxazole (100 mg/L) and sodium diclofenac (50 mg/L) solutions were prepared by adding the corresponding solid to water. Quantification of adsorbates was performed by UV–VIS spectroscopy at 229 and 264 nm for SMX and DF, respectively, using a Jasco U 560 UV–VIS Jenway 7315 spectrophotometer. The calibration curves were obtained from the analysis of the spectra obtained at distinct concentrations: SMX (0.1–50.0 mg/L) and DF (0.05–50 mg/L) with good linearity in both cases ($R^2 > 0.992$) (Figure S1). Adsorption experiments were obtained with a batch equilibration procedure using 15 mL polypropylene centrifuge tubes covered with polypropylene caps immersed in a thermostatic shaker bath in which the exact amount of adsorbent (5 mg/mL dosage) was placed in contact with solutions with known SMX and DF concentration. The mixtures were shaken at room temperature, and aliquots of 1 mL were collected along the time (for 24 h). The amount of drug adsorbed per mass unit at each time t (q_t, mg/g) was determined by equation (1), and the percentage removal was calculated using equation (2):

$$q_t = (C_o - C_t) \times \frac{V}{m}(1), R(\%) = \frac{C_o - C_t}{C_o} \times 100 \quad (2)$$

where C_o (mg/L) is the initial concentration (mg/L), C_t (mg/L) is the drug concentration in the aqueous phase at time t (min), V (L) is the volume of solution, and m (mg) is the mass of the adsorbent. Equilibrium isotherms for the removal of SMX and DF were obtained with different concentrations at the natural pH of each solution and 25 °C for 24 h.

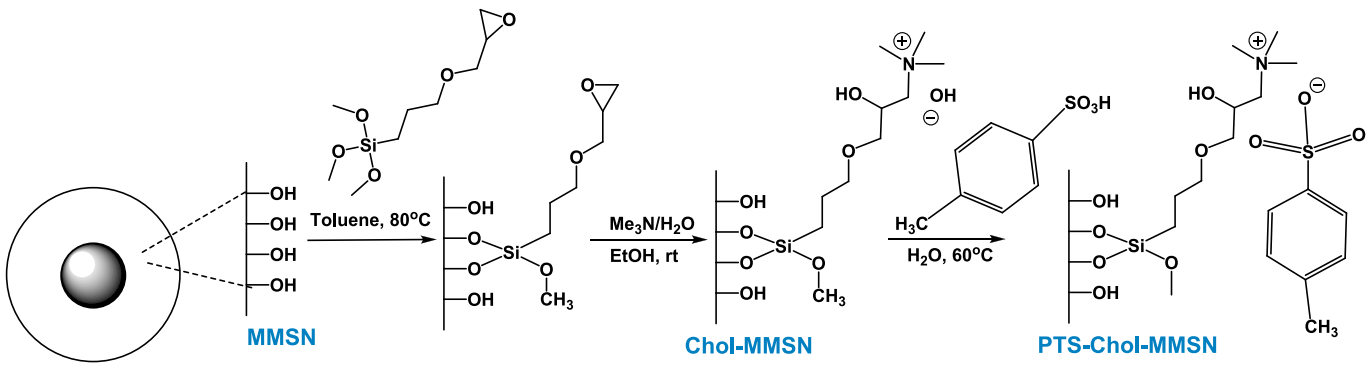

Scheme 1. Immobilization of choline hydroxide and choline p-methyl toluene sulfonate functionalities onto magnetic mesoporous silica nanoparticles.

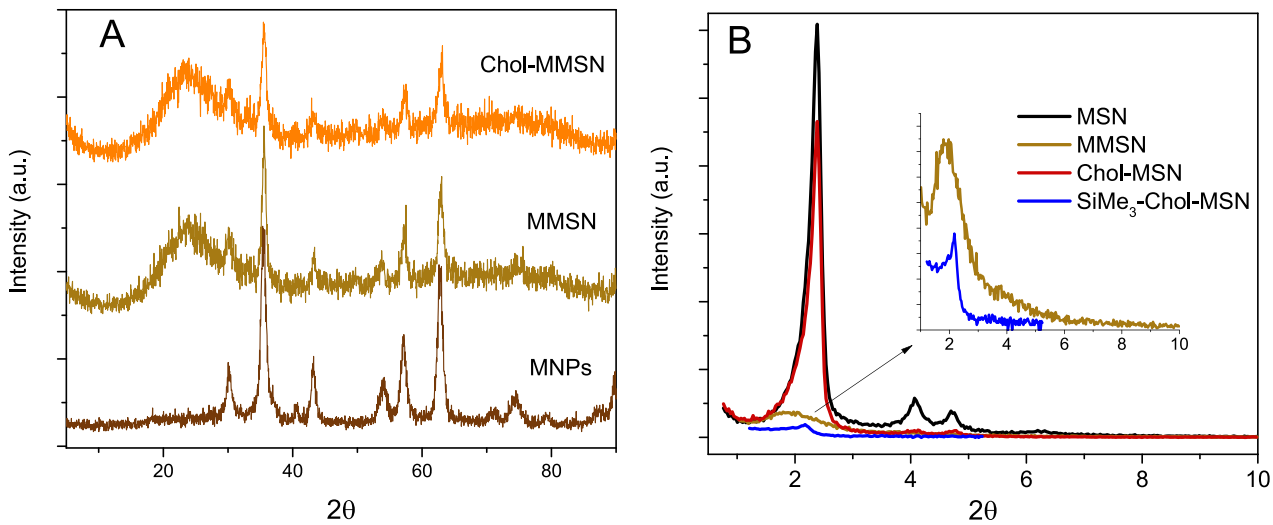

Fig. 1. High-angle XRD patterns of MNPs, MMSN, and Chol-MMSN (A) Small-angle XRD patterns of MMSN, MSN, Chol-MSN, and $SiMe_3$-Chol-MSN (B).

2.4. Characterization

This work has been carried out by using several characterization techniques, such as X-ray diffraction (XRD), X-ray fluorescence (XRF), adsorption–desorption isotherms of N_2, DRUV–vis, thermogravimetric analysis (TGA), solid-state ^{13}C NMR, TEM, and zeta potential, contact angle and electrochemical measurements. The equipment used and the measurements' conditions followed have been fully described in the supplementary material.

3. Results and discussion

3.1. Synthesis and characterization of the adsorbent materials

Mesoporous silica-coated core–shell magnetite nanoparticles (MMSN) were synthesized using a surfactant-templated sol–gel method. The process involved utilizing MNPs (Fe_3O_4, magnetic nanoparticles) stabilized with tetramethylammonium hydroxide as nucleation seeds. This approach helped reduce the average particle size and enabled the production of a highly stable magnetic fluid, as these particles could be easily dispersed in aqueous media. The use of CTAB as the surfactant, TEOS as a silicon source, and triethanolamine as a basic initiator of the sol–gel process allows the formation of a mesoporous silica layer around the Fe_3O_4 core (MNPs). The template is removed by calcination to yield MMSN, which has been used as support to prepare hybrid materials with two different functionalities: choline hydroxide, and choline p-methyl toluene sulfonate. We synthesized a silane ligand containing the choline hydroxide functionality by reacting 3-glycidyloxypropyltrimeth oxysilane with trimethylamine. This reaction allows for the opening of the epoxide ring and subsequent quaternization of the amine group. To do so the epoxide silane ligand is firstly anchored to the silica surface of MMSN in a straight and well-known reaction followed by the reaction with trimethylamine. The material will be identified as Chol-MMSN from now on.

This functionality can be easily modified by a straightforward acid-base reaction using an aqueous solution of methyl p-toluene sulfonic acid, resulting in a new choline methyl p-toluene sulfonate functionality (PTS-Chol-MMSN) (Scheme 1). For comparison purposes, to investigate the influence of porous architecture on the adsorption process, hybrid materials Chol-MSN and PTS-Chol-MSN based on mesoporous silica nanospheres (MSN) have been also synthesized using similar procedures.

To mask the unreacted silanol groups in the hybrid mesoporous silicas, which have the potential to form hydrogen bonds with many drugs, a reaction with hexamethyldisilazane was employed. This led to the formation of two additional amphipathic materials namely $SiMe_3$-Chol-MSN and PTS-$SiMe_3$-Chol-MSN, which possess hydrophobic -$SiMe_3$ groups on the silica surface in addition to the choline hydroxide and choline methyl p-toluene sulfonate functionalities. This approach aims to comprehend the effects of different functionalities and elucidate the role of silanol groups in the adsorption mechanism.

The crystalline nature of the materials was determined by X-ray

Table 1
Textural properties of some representative materials under study.

	Surface area (m^2g^{-1})	Pore volume (cm^3g^{-1})	Pore size (Å)
MNPs	104	0.42	*
MMSN	727	0.60	29
MSN	1042	0.96	37
Chol-MMSN	414	0.42	27
Chol-MSN	825	0.50	24
PTS-Chol-MSN	234	0.25	19
$SiMe_3$-Chol-MSN	239	0.26	18

*Pore size measured, 250 Å, is due to the interparticle space between nanoparticles [34].

diffraction. Fig. 1A shows the wide-angle XRD patterns of MNPs, core–shell MMSN, and hybrid Chol-MMSN. For MNPs six characteristic peaks corresponding to planes of magnetite, a cubic inverse spinel, are observed. The peak broadening of XRD patterns of Fe_3O_4 indicates the significantly small size of the resulting crystallites. The average crystallite size calculated using Scherrer's equation is 9.7 nm. The crystalline structure of MMSN, after magnetite nanoparticles coating with mesoporous silica, is retained showing that the embedded MNPs maintain their structure after workup and template calcination. The mesostructure of all MMSN-based materials was confirmed by small-angle XRD, the materials show a well-resolved pattern at low 2θ values with one (1 0 0) diffraction peak at 1.90 (See Fig. 1B). The low intensity of the (1 0 0) plane in comparison to MSN-based materials and non-existent additional high order peaks (1 1 0) and (2 0 0), characteristics of ordered hexagonal mesoporous silica, are attributed to the low local order, due to variations in the wall thickness of the framework and the reduction of scattering contrast between the channel wall and the ligands present on the inner surface of silica materials.

The physical parameters such as the surface area (S_{BET}), total pore volume, and BJH average pore diameter have been measured by nitrogen adsorption experiments and are summed up in Table 1. The characteristic type IV BET isotherms for the prepared materials show the presence of mesoscale pores (Figs. 2 and S2). The sharp N_2 condensation

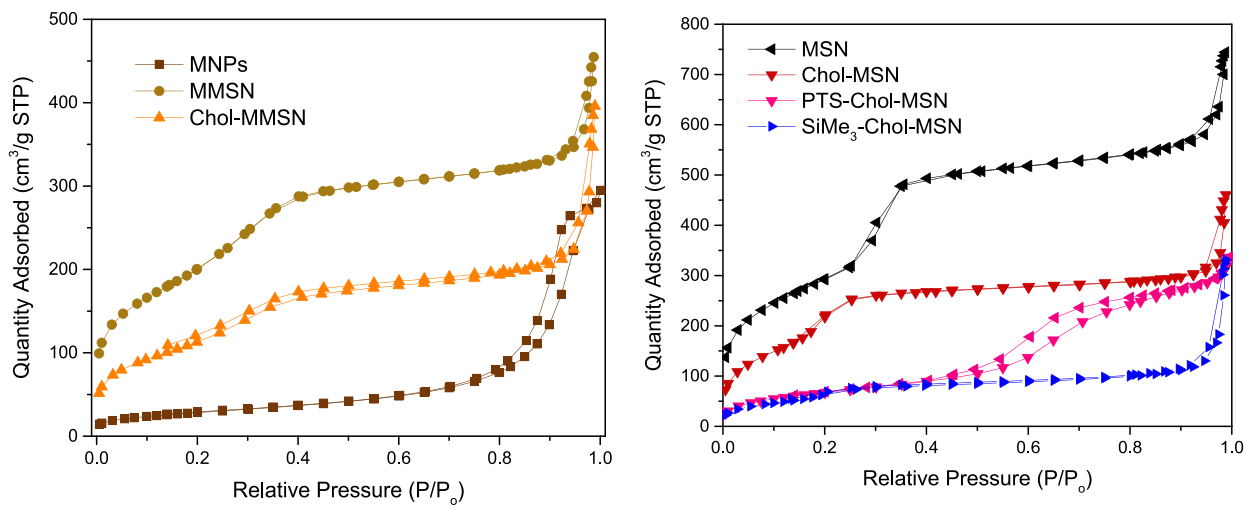

Fig. 2. Nitrogen adsorption/desorption isotherms of synthesized materials.

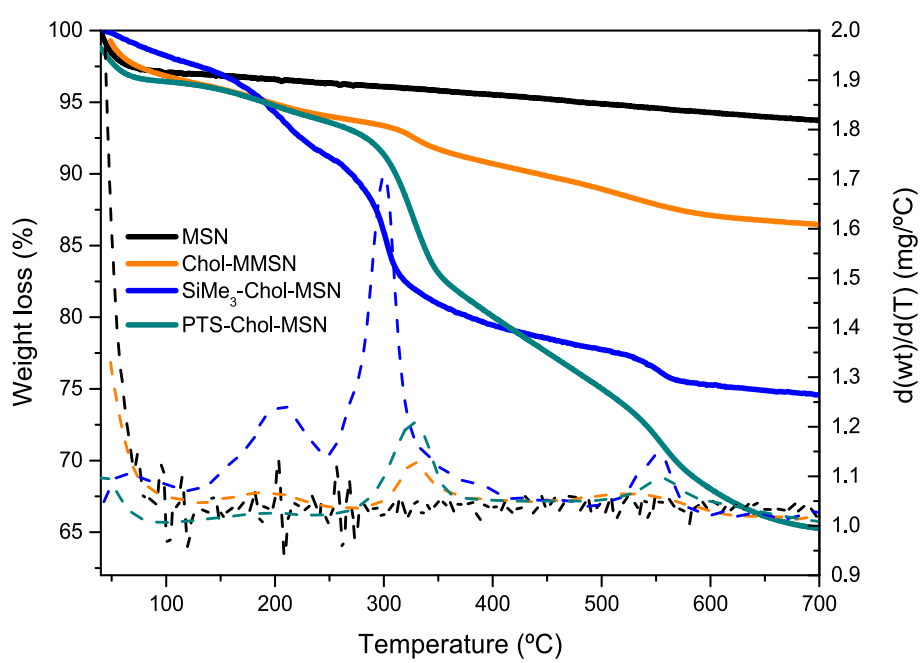

Fig. 3. Thermogravimetric analysis of some representative adsorbent materials.

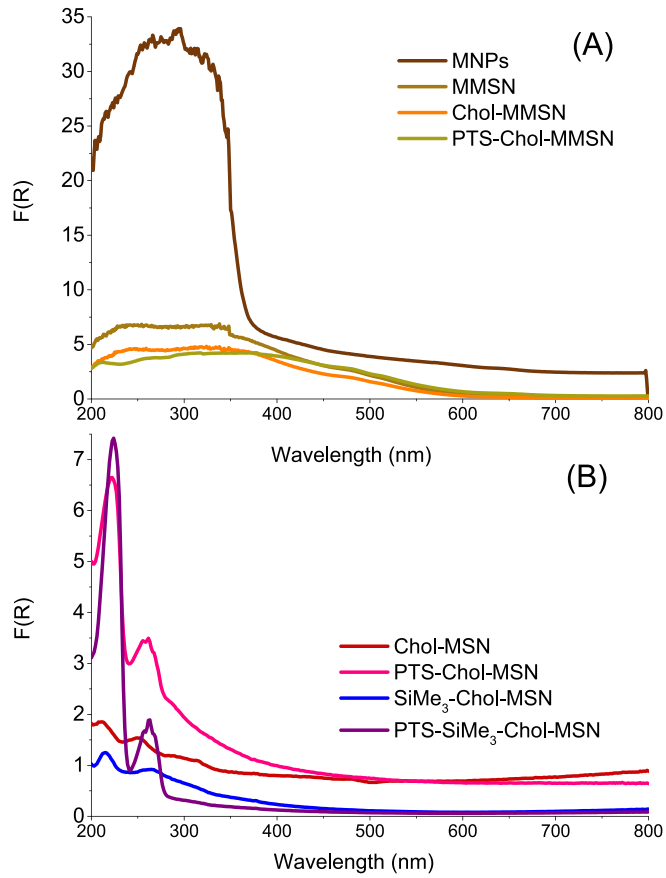

Fig. 4. DRUV–vis spectra of MNPs, MMSN, Chol-MMSN, PTS-Chol-MMSN materials (A), and their counterparts based on MSN (B).

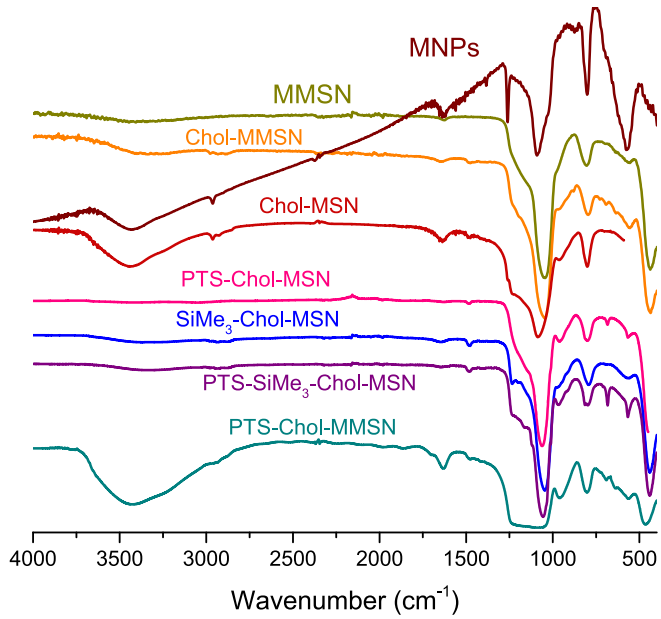

Fig. 5. FTIR spectra of MNPs, MMSN, Chol-MMSN, PTS-Chol-MMSN materials and their counterparts based on MSN.

step at $P/P_o = 0.2–0.4$ for MSN and MMSN type materials indicates that the supports have a highly ordered hexagonal pore system. The pristine MMSN material possesses S_{BET} (727 m^2 g^{-1}), a pore volume of 0.60 cm^3 g^{-1}, and a BJH pore diameter of 29 Å. The hybrid material Chol-MMSN presents an important reduction in the S_{BET}, (414 m^2 g^{-1}), pore volume (0.42 cm^3 g^{-1}), and average BJH pore diameter (27 Å) in comparison with the parent support. This decrease is due to the presence of choline hydroxide functionality anchored to the channels which partially block the adsorption of nitrogen molecules. An additional capillary condensation step above $P/P_0 > 0.9$ is observed, suggesting the formation of interparticle porosity and the increase in aggregation. As expected, MSN and hybrid Chol-MSN systems show higher surface area, pore volume, and pore size in comparison with their magnetic counterparts. PTS-Chol-MSN shows a predictable decrease in textural properties upon functionalization with the sterically demanding methyl-p-toluene sulfonate. Finally, the textural property values obtained for $SiMe_3$-Chol-MSN demonstrate that the silylation process takes place efficiently, resulting in significant decreases in surface area and pore volume compared to the unsilylated sample, Chol-MSN.

Thermogravimetric measurements were performed for some representative materials. Chol-MMSN TGA shows a significant total weight loss of 10.5 %. The weight loss between 25 °C and 100 °C can be attributed to physisorbed water (Fig. 3). The subsequent losses between 150 and 400 °C are attributed to the silane ligand based on the choline unit. Based on the 5.8 % weight loss in the range 150 °C and 400 °C the ligand loading is estimated at 0.24 mmol g^{-1}. Based on the nitrogen content obtained by elemental analysis the number of ligand molecules attached to the support in Chol-MMSN was calculated to be 0.34 mmol g^{-1} (L_o = %N/nitrogen molecular weight). TGA for $SiMe_3$-Chol-MSN shows a total weight loss of 22 % between 150 °C and 400 °C which is in accordance with the presence of trimethylsilyl groups capping the silica surface besides the choline functionality. PTS-Chol-MSN shows a similar weight loss of 20 % between 150 °C and 400 °C which is explained by the highest size of the methyl p-toluene sulfonate functionality. Considering L_o and S_{BET} of the magnetic mesoporous silica nanoparticles, the average surface density, d, of attached molecules and the average intermolecular distance are calculated to be 0.19 molecules/nm^2 and 2.27 nm, respectively. Similarly, based on the sulfur content obtained by XRF measurement the number of methyl p-toluene sulfonate anions attached to the support in PTS-Chol-MMSN is 0.04 mmol g^{-1}, this data suggests that the acid-base reaction between p-toluene sulfonic acid and choline hydroxide moiety is not quantitative and hence both functions may coexist in the hybrid materials PTS-Chol-MMSN and PTS-Chol-MSN.

To study the iron core coating process and subsequent ligand immobilization DRUV–vis spectra of pristine and hybrid materials were also recorded. The diffuse reflectance DRUV–vis spectrum of magnetite nanoparticles shows a strong absorption envelope centered at 345 nm, which represents transitions between the oxygen non-bonding and metal d-orbitals (VB*to CF) of both octahedral and tetrahedral ions. The main characteristic in DRUV–vis spectra of silica core–shell nanoparticle materials is the important decrease of absorbance intensity due to the loading of the iron core by a layer of mesoporous silica. The weak absorption bands due to the hydroxide choline functionality expected around 210 and 250 cm^{-1}, as observed in Chol-MSN, are completely overlapped by the broadband attributed to the iron core. Similarly, the absorption bands due to the methyl p-toluene sulfonate group at 222 and 260 nm are seen in PTS-Chol-MSN and as expected, overlapped in PTS-Chol-MMSN, although the absorption band at 222 nm can be inferred included in the total envelope (Fig. 4).

The FTIR spectra of pristine MMSN and MSN show characteristic bands at 3441 cm^{-1} assigned to O–H stretching vibrations and the remaining physisorbed water molecules, at 1629 cm^{-1} due to deformation vibrations of the adsorbed water molecules and at 1082, 959, and 806 cm^{-1} attributed to the Si-O stretching vibrations. The incorporation of choline-based functionality Chol-MMSN and Chol-MSN adds new bands to the spectra corresponding to ν(C–H) stretching vibrations at 2937 and 2881 cm^{-1} and two nearby bands at 1487 and 1476 cm^{-1} attributed to the bending vibrations of δ(C–H) of the tetraalkylammonium group of the choline unit. When comparing with PTS-Chol-MMSN and PTS-Chol-MSN no significant differences are found since the

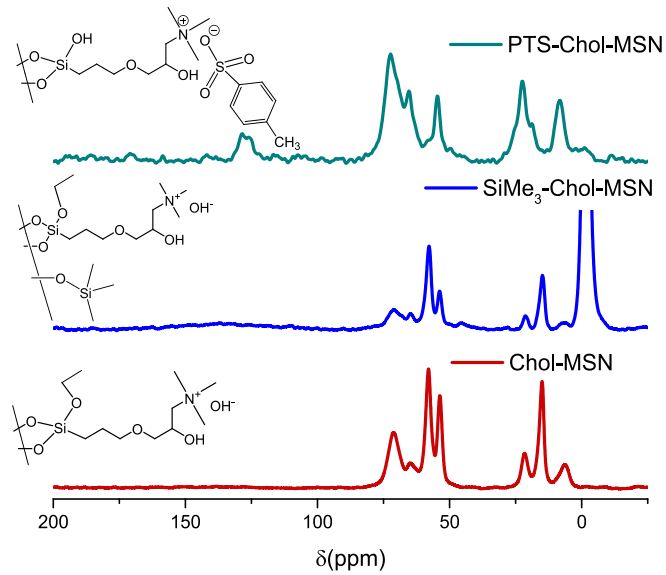

Fig. 6. ^{13}C CP MAS NMR of Chol-MSN, $SiMe_3$-Chol-MSN and PTS-Chol-MSN.

stretching bands associated with the $\nu(O = S = O)$ group are expected around 1190 and 1130 cm^{-1} (asymmetric) and 1040 cm^{-1} (symmetric) and appear completely overlapped with the silica bands. However, the peak attributed to the stretching vibration of the C − S bond appears at 683 cm^{-1}. In addition, in the silylated materials new bands are observed due to the incorporation of end-capping trimethylsilyl ligands. $SiMe_3$-Chol-MSN shows a signal at 845 cm^{-1} assigned to the Si–CH_3 antisymmetric deformation stretch. Both the silylated and unsilylated silicas display a silanol band in the region of 3700–3200 cm^{-1}. However, the silylated material showed a very significant decrease in the silanol band (Fig. 5). This result is mainly due to the conversion of silanol to trimethylsilyl groups, but it is also likely to be due to diminished water adsorption from an increase in hydrophobicity.

As representative samples and since the ligand loading is higher in MSN-based materials, the ^{13}C CP MAS NMR spectra of Chol-MSN, PTS-Chol-MSN, and silylated $SiMe_3$-Chol-MSN have been recorded (See Fig. 6). The spectrum of Chol-MSNs exhibits signals at 6, 22, and 71 ppm due to the carbon atoms of the propyl chain -Si-CH_2-, –CH_2-CH_2-CH_2- and –CH_2-CH_2-CH_2-O, respectively. The signal attributed to the methylene group O-CH_2-CHOH- appears at 71 ppm (overlapped) and the signals due to carbon atoms of the opened epoxide function appear at 66 and 72 ppm, the methine *C*H-OH and methylene N–CH_2– groups, respectively. Two additional peaks at 15 and 59 ppm are assigned to the ethoxide group of the organic ligand CH_3CH_2-O- bonded to silica, which suggests the interchange of the methoxide group present in the original (glycidyloxypropyl)trimethoxysilane used as reactant and ethanol used as the solvent. The resonance peak at ca. 54 ppm indicates the presence of methyl groups attached to the nitrogen in the quaternary ammonium group. The spectrum of silylated $SiMe_3$-Chol-MSN is similar but in addition, shows an intense signal at −1.8 ppm due to the $SiMe_3$ groups. Finally, the ^{13}C CP MAS NMR spectrum of PTS-Chol-MSN obtained after reaction in aqueous media with methyl p-toluenesulfonic acid shows a similar pattern of signals for the choline unit and further signals attributed to the methyl p-toluene sulfonate unit CH_3-C_6H_4-SO_3^-. The methyl group attached to the aromatic ring appears at 19 ppm, and the carbon atoms of the aromatic ring CH_3-C_6H_4-SO_3^- resonate at 125, 128, and 141 ppm.

TEM images of MNPs and MSN are shown in Fig. 7A and C, respectively. Crystallite size's MNPs agrees with that predicted by the Scherrer equation, and MSN which are uniform in shape show a size diameter of around 75 nm. MMSN TEM's image in Fig. 7B shows that magnetite cores turn up encapsulated by mesoporous silica. In addition, as

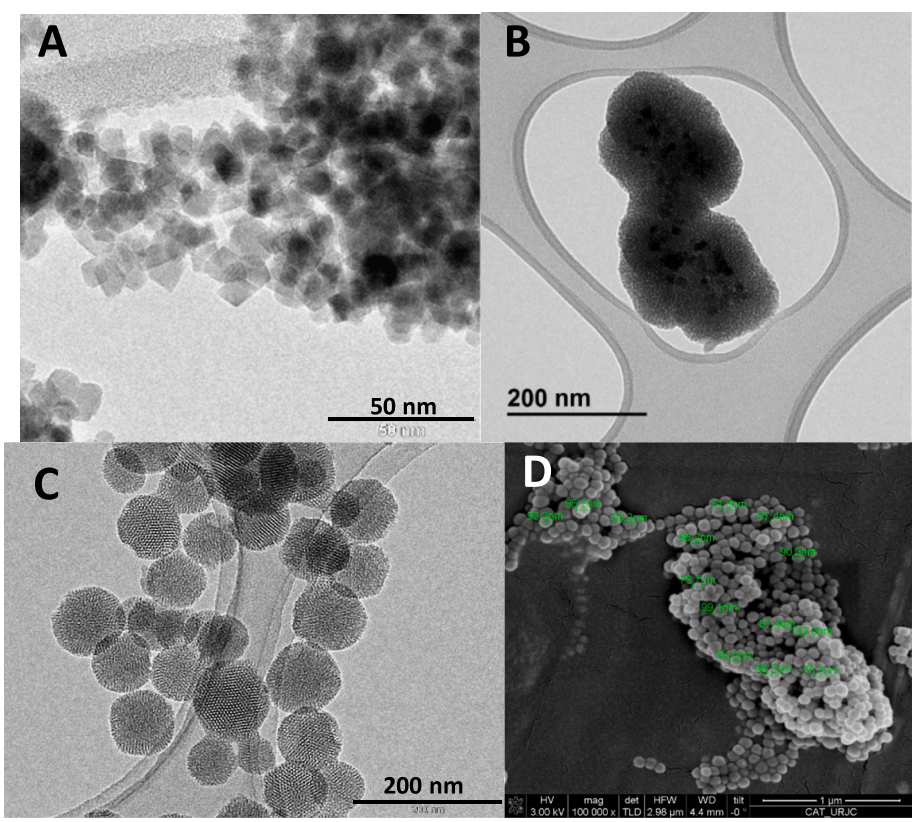

Fig. 7. TEM images of (A) magnetic nanoparticles, MNPs (B) spherical core–shell MMSN, (C) mesoporous silica nanoparticles, MSN, and (D) SEM micrographs of spherical core–shell MMSN nanoparticles.

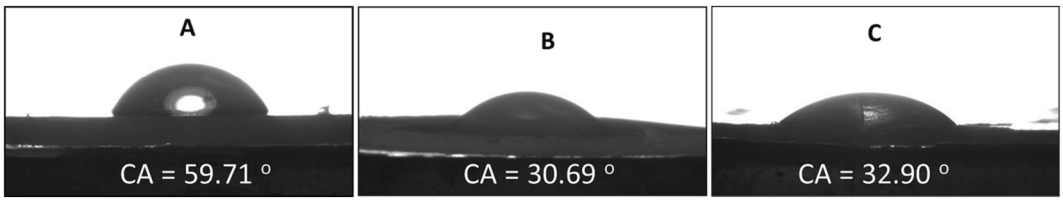

Fig. 8. The contact angle of water on the surface of (A). $SiMe_3$-Chol-MSN, (B) Chol-MSN and (C) PTS-$SiMe_3$-Chol-MSN.

Table 2
Batch adsorption experiments were carried out by using 5 mg of adsorbent and 5 mL of 50 ppm of adsorbate solution during 24 h at room temperature.

Entry	Adsorbent	ζ-potential (eV)	Drug	q_t (mg/g)	R (%)
1	MMSN	−4.1	DF (pH 5)	2.1	3.9
2	Chol-MMSN	36.0	DF (pH 3)	81.9	91.5
3	Chol-MMSN	13.1	DF (pH 5)	6.2	6.4
4	Chol-MMSN	−3.2	DF (pH 7)	2.8	2.9
5	PTS-Chol-MMSN	11.5	DF (pH 5)	41.5	82.4
6	Chol-MSN	18.7	DF (pH 5)	7.9	7.9
7	PTS-Chol-MSN	15.4	DF (pH 5)	80.7	94.8
8	$SiMe_3$-Chol-MSN	24.7	DF (pH 5)	6.5	7.0
9	PTS-$SiMe_3$-Chol-MSN	17.8	DF (pH 5)	61.3	67.7
10	Chol-MSN	35.3	SMX (pH 3)	8.0	6.4
11	Chol-MSN	18.7	SMX (pH 5)	13.2	10.4
12	Chol-MSN	−4.8	SMX (pH 7)	2.9	2.3
13	PTS-Chol-MSN	15.4	SMX (pH 5)	27.2	51.0
14	PTS-Chol-MMSN	11.5	SMX (pH 5)	13.1	25.0
15	$SiMe_3$-Chol-MSN	24.7	SMX (pH 5)	4.4	4.5
16	PTS-$SiMe_3$-Chol-MSN	17.8	SMX (pH 5)	4.8	4.9

previously predicted by N_2 adsorption–desorption isotherms, a high aggregation of nanoparticles is observed. The morphological characterization of the Chol-MMSN performed by SEM (Fig. 7D) shows the homogeneous distribution and the spherical shape of nanoparticles with a size of around 90 nm.

3.2. Adsorption experiments

This study focuses on evaluating a family of hybrid mesoporous silica materials as adsorbents for two different drugs. Various variables have been investigated to determine their adsorbent properties so efficient materials could be designed for this purpose. To begin with, we have investigated the impact of the support by comparing mesoporous silica nanospheres (MSN) with core–shell magnetic mesoporous silica nanospheres (MMSN). While MMSN nanoparticles offer the advantage of being easily recoverable (See Figure S7), MSN nanoparticles exhibit higher BET surface area, pore volume, and pore size making them more advantageous for adsorption experiments.

Secondly, two different alkoxy silane ligands with the cationic choline functionality have been employed to modify the silica surface. The ligands differ in their counterions: hydroxide in Chol-MSN and Chol-MMSN and, methyl p-toluene sulfonate in PTS-Chol-MMSN and PTS-Chol-MSN. Furthermore, the influence of the silanol groups on the silica surface has been also tested by preparing $SiMe_3$-Chol-MSN and PTS-$SiMe_3$-Chol-MSN. In these materials, the silanol groups on the silica surface have turned into the hydrophobic trimethylsilyl groups, resulting in the formation of amphipathic materials.

Wettability experiments were conducted to assess the surface properties of the materials. On the surface of $SiMe_3$-Chol-MSN, a water droplet exhibited a contact angle (CA) of 59.71 degrees, indicating poor wettability of the material towards water. Similarly, a water droplet was placed on the surface of Chol-MSN and a contact angle of 30.69 degrees was measured which suggests a lower surface hydrophobicity compared to sylilated $SiMe_3$-Chol-MSN. Furthermore, contact angle analysis was

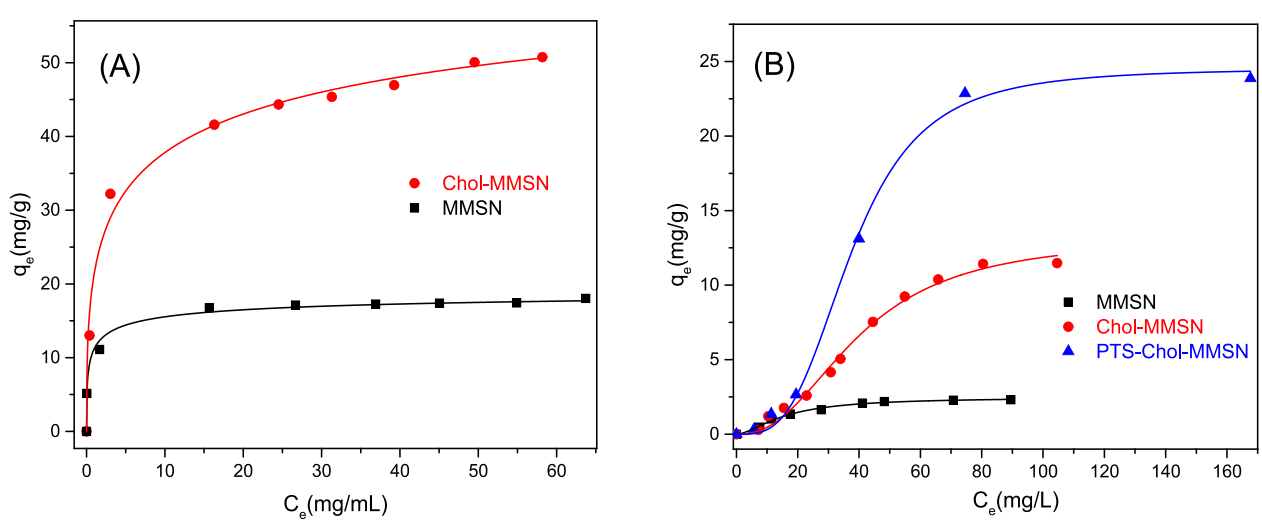

Fig. 9. Adsorption Isotherm data for (A) DF and (B) SMX and Sips model fitting (full line) with different adsorbents. Condition: 5 mg of adsorbents in 5 mL solution, in a range of concentrations at 25 °C.

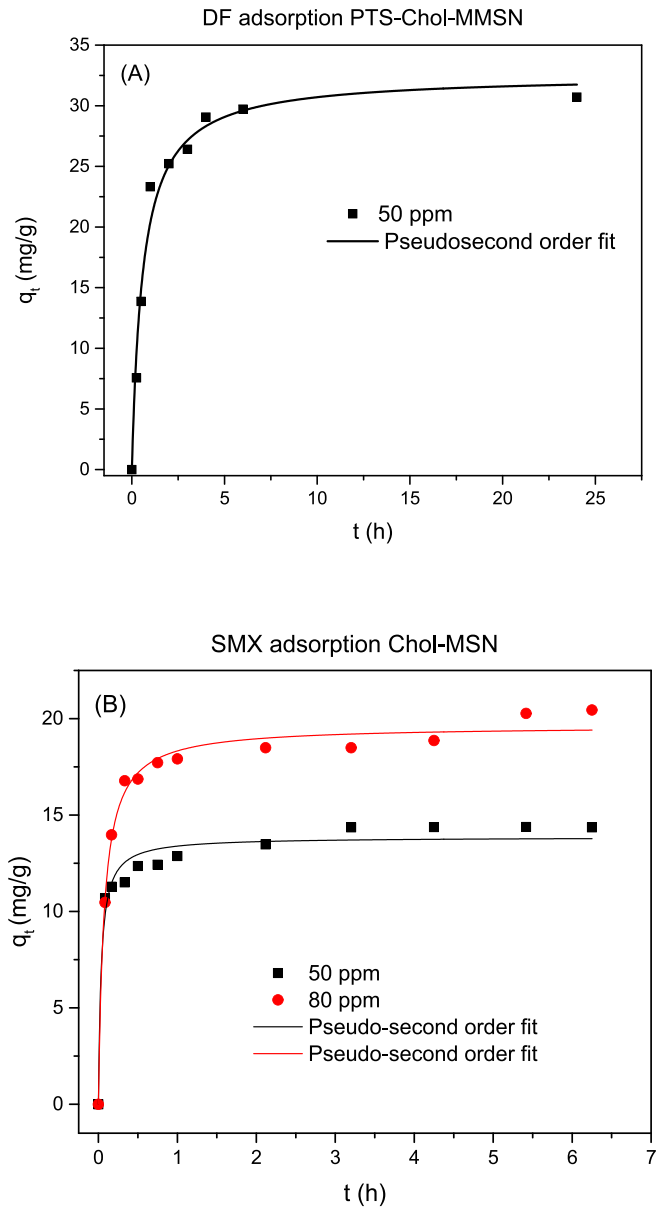

Fig. 10. Effect of contact time on (A) DF adsorption over PTS-Chol-MMSN and (B) SMX over Chol-MSN. Conditions: 5 mg of adsorbent in 5 mL solution, 1–24 h at 25 °C.

performed on the surface of PTS-$SiMe_3$-Chol-MSN. When water droplets were placed on the solid surface, the contact angle measured was 32.90 degrees, indicating good hydrophilicity after the incorporation of methyl p-toluene sulfonate in comparison to $SiMe_3$- Chol-MSN (Fig. 8). This suggests that the presence of methyl p-toluene sulfonate leads to enhanced hydrophilic properties of the material.

For this study, two drugs with different properties were chosen. Sulfamethoxazole (SMX) is an amphoteric polar compound belonging to the sulphonamide antibiotics family. It is a high molecular weight molecule with high solubility in water. Due to its high solubility, SMX exhibits a low affinity for solid surfaces, resulting in low solid–liquid distribution coefficients (K_d), which explains its mobility in soils and its occurrence and transport in natural waters. As a result, SMX is not efficiently removed by conventional biological treatments in wastewater and may persist in the environment for more than a year [25]. The protonation states of SMX are pH-dependent, which significantly affects its reactivity. Their pK_a values are $pK_{a1} = 1.6$ and $pK_{a2} = 5.7$, that is, below pH 1.6, SMX is in its cationic form, while above pH 5.7, it exists in its anionic form (See Figure S8). On the other hand, diclofenac (DF) behaves as a weak acid compound with a pk_a value of 4.00. At pH values below the pk_a, DF is mainly protonated, whereas, at pH values above the pk_a, it becomes deprotonated and carries a negative charge. Related to pH, the isoelectric point (IEP) is the pH at which a molecule carries no net electrical charge or is electrically neutral in the statistical mean. SMX molecule, in its zwitterionic form, is neutral at pH = IEP (around a range of pH 2–5), and DF shows a neutral charge at pH values below its pK_a (pH < 4). DF is also a non-polar compound sparingly soluble in water due to its intrinsic hydrophobicity. The carboxylic group in the non-ionized form of DF participates in the formation of dimers through hydrogen bonds, which results in limited interaction with water molecules. Therefore, pH has a significant impact on the surface chemistry of the adsorbent, and on the speciation of solutions, and plays a crucial role in the interactions at the adsorbent–adsorbate interface.

Measurement of ζ potential for the adsorbent material as a function of pH provides valuable information about the surface charge of the adsorbent. Pristine silicas as MSN and MMSN reach the isoelectric point between pH 2–3, where the negative and positive charges created by the silanol groups are balanced. At this point, the silanol groups ≡Si-OH are stable. As the pH value increases above 4, the ζ potential becomes increasingly negative, indicating a greater negative charge on the particle surface and an abundance of $\equiv Si\text{-}O^-$ [26].

Measurements of ζ potential for Chol-MSN and Chol-MMSN materials show comparable values, as expected. The isoelectric point is reached between pH 6 and 7 (Table 2), which means that at pH not higher than 6 the surface is positively charged due to the presence of the quaternary ammonium groups from the choline unit present at the particles' surface. These positively charged groups can interact electrostatically with deprotonated species. At higher pH values, the ζ potential becomes more negative, likely due to the abundance of $\equiv Si\text{-}O^-$ species on the silica surface, resulting in repulsive interactions with the drugs under study.

PTS-Chol-MSN reaches the isoelectric point above neutral pH, which implies that the nature of the anion influences the electrostatic interactions with deprotonated species (ζ potential = 1.8 at pH 7 and Table 2). Lastly, silylated materials $SiMe_3$-Chol-MSN (ζ potential = 23.1 at pH 7) and PTS-$SiMe_3$-Chol-MSN (ζ potential = 9.1 at pH 7) exhibit the highest ζ potential values at pH 5. This can be attributed to the absence of $\equiv Si\text{-}O^-$ species which are substituted by $\equiv Si\text{-}O\text{-}SiMe_3$. The surface charge of the adsorbents, along with the presence or absence of silanol groups capable of forming hydrogen bonds with the adsorbates, plays a crucial role in understanding the adsorption mechanism.

Table 2 displays the results of batch adsorption experiments carried out using 5 mg of adsorbent and 5 mL of a 50 ppm of adsorbate solution for 24 h at room temperature. The data reveals the impact of functionalization on the adsorption of DF by Chol-MMSN which increases DF adsorption threefold in comparison to naked silica MMSN (entries 1 and 3). The adsorption of DF by Chol-MMSN is strongly influenced by the ζ potential, making it pH-dependent. At pH 3, Chol-MMSN exhibits a high q_t value of 81.9 mg/g, indicating favourable adsorption conditions (Entry 1). However, as the pH gradually increases from 3 to 7 (Entries 2–4), the DF adsorption capacity diminishes, likely due to a decrease in the surface charge of the nanoparticles, which was confirmed by the ζ potential data. At pH 7, DF carries a negative charge, potentially leading to repulsive interactions with the negatively charged Chol-MMSN surface. However, the adsorption is not negligible at this pH suggesting that electrostatic interactions are not the sole governing mechanisms of the adsorption process. At pH 5, higher adsorption of SMX by Chol-MSN is observed (Entries 10–12, $q_t = 13.2$ mg/g). At this pH, the silica particles are positively charged, DF is in its deprotonated form, and SMX is either neutral or in the zwitterion form. In both cases, this promotes electrostatic interactions and increases the adsorption capacity of hybrid mesoporous silicas.

The practical considerations of using very acidic pH values, along with the fact that DF adsorption is not solely driven by electrostatic

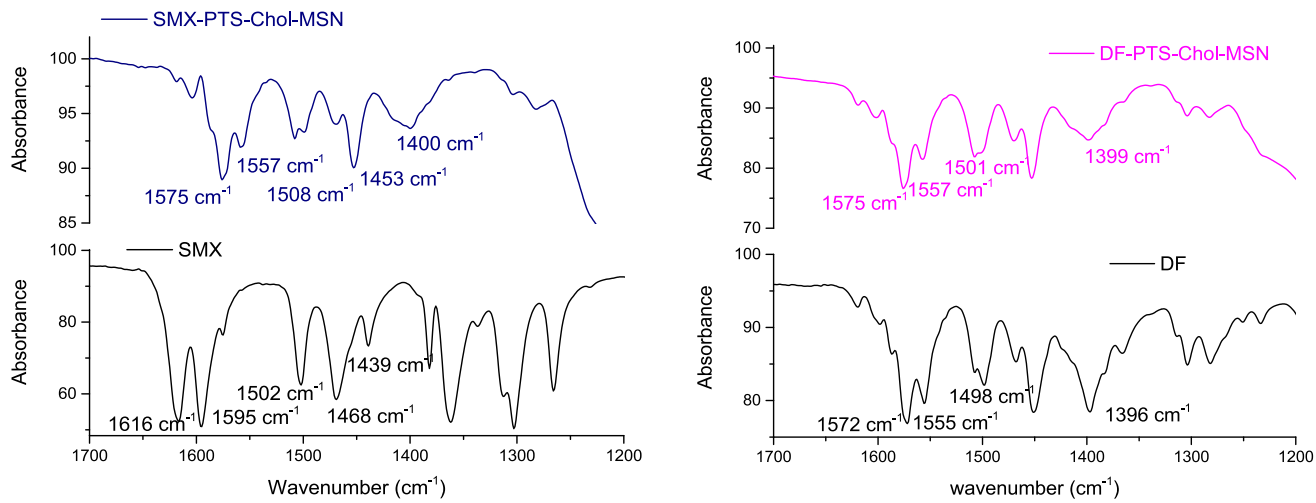

Fig. 11. FTIR spectra of PTS-Chol-MSN adsorbent after SMX (left plot) and DF (right plot) adsorption procedure in comparison to free drugs.

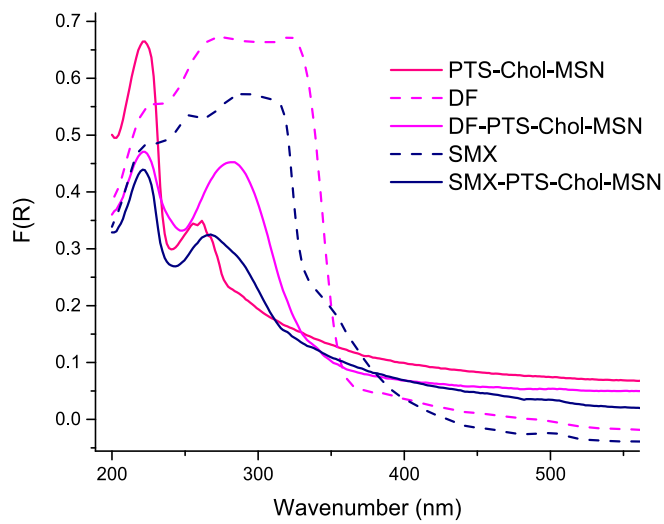

Fig. 12. DR-UV–vis spectra of PTS-Chol-MSN adsorbent after SMX and DF adsorption procedure in comparison to free drugs.

interactions, have led us to the selection of pH values 5 and 7 for the remaining experiments. These pH values are similar to those obtained when the drugs are dissolved in pure water, which typically results in a pH of around 5–6.

When comparing the functionalities used as active sites, SMX exhibits a higher affinity for the hybrid silica with the methyl p-toluene sulfonate anion, PTS-Chol-MSN, compared to the silica with the hydroxide anion, Chol-MSN. The adsorption capacity (q_t) of SMX is doubled in PTS-Chol-MSN (q_t = 27.2 mg/g) compared to Chol-MSN (q_t = 13.2) (Entries 11 and 13). Similarly, DF demonstrates an even stronger affinity for PTS-Chol-MMSN, with a nearly sixfold increase in q_t compared to Chol-MMSN. The q_t value for DF is significantly higher in PTS-Chol-MMSN (q_t = 41.5 mg/g) compared to Chol-MMSN (q_t = 6.2 mg/g) (Entries 4 and 5).

The surface area of the adsorbents is another important variable to consider. As expected, the higher surface area of PTS-Chol-MSN compared to PTS-Chol-MMSN results in increased adsorption of DF (from q_t = 41.5 to 80.7 mg/g) (Entries 5 and 7). Similarly, the adsorption of SMX is also enhanced by the higher surface area of PTS-Chol-MSN, resulting in a higher q_t value (from q_t = 13.1 to 27.2 mg/g). Lastly, when comparing the q_t values obtained for the best adsorbent, PTS-Chol-MSN, it can be concluded that DF is efficiently removed from water with a removal efficiency (% R) of 94.8 %, while SMX is promising recovery with an % R of 51 % (Entries 7 and 13).

The influence of silanol groups on the silica surface was also investigated. As observed earlier, the presence of silanol groups has an impact on the surface charge of the adsorbents at different pH values, which affects the establishment of electrostatic interactions between the adsorbent and the adsorbate. Additionally, the ≡Si-O–H groups present in the silanol groups can engage in hydrogen bonding with the oxygen atoms, amines, carbonyl groups, and carboxylate groups available in the DF and SMX molecules [27].

The higher adsorption values of DF and SMX measured for Chol-MSN compared to its silylated counterpart $SiMe_3$-Chol-MSN (Entries 6 and 8, and 11 and 15), as well as for PTS-Chol-MSN compared to PTS-$SiMe_3$-Chol-MSN (Entries 7 and 9, and 14 and 16), demonstrate that the presence of silanol groups is a critical factor in the adsorption process. Despite the higher ζ potential observed for the silylated materials at the studied pH values, the data indicate that the interactions between the adsorbent and the adsorbate primarily depend on the formation of hydrogen bonds with the functional groups present in the organic molecules. Consequently, the subsequent experiments will be conducted using the most efficient non-silylated materials.

The effect of adsorbent dosage was investigated by conducting experiments using different amounts of Chol-MMSN. Three dosages were tested: 1, 2, and 5 g/L (corresponding to 5, 10, and 25 mg of adsorbent in 5 mL of a 25 ppm DF solution), with a contact time of 24 h at room temperature. As expected, the removal efficiency of DF was significantly enhanced with an increase in adsorbent dosage, as more active sites were available for adsorption. However, this increase was not linear, indicating that the active sites were not equally accessible to the solute at higher adsorbent dosages. The influence of temperature was also examined by experimenting with the highest adsorbent dosage at 37 °C. The results showed a significant reduction in the removal efficiency, nearly halving the effectiveness compared to room temperature (See Figure S3). This suggests that the adsorption process is temperature-dependent, with lower temperatures favoring higher removal efficiencies.

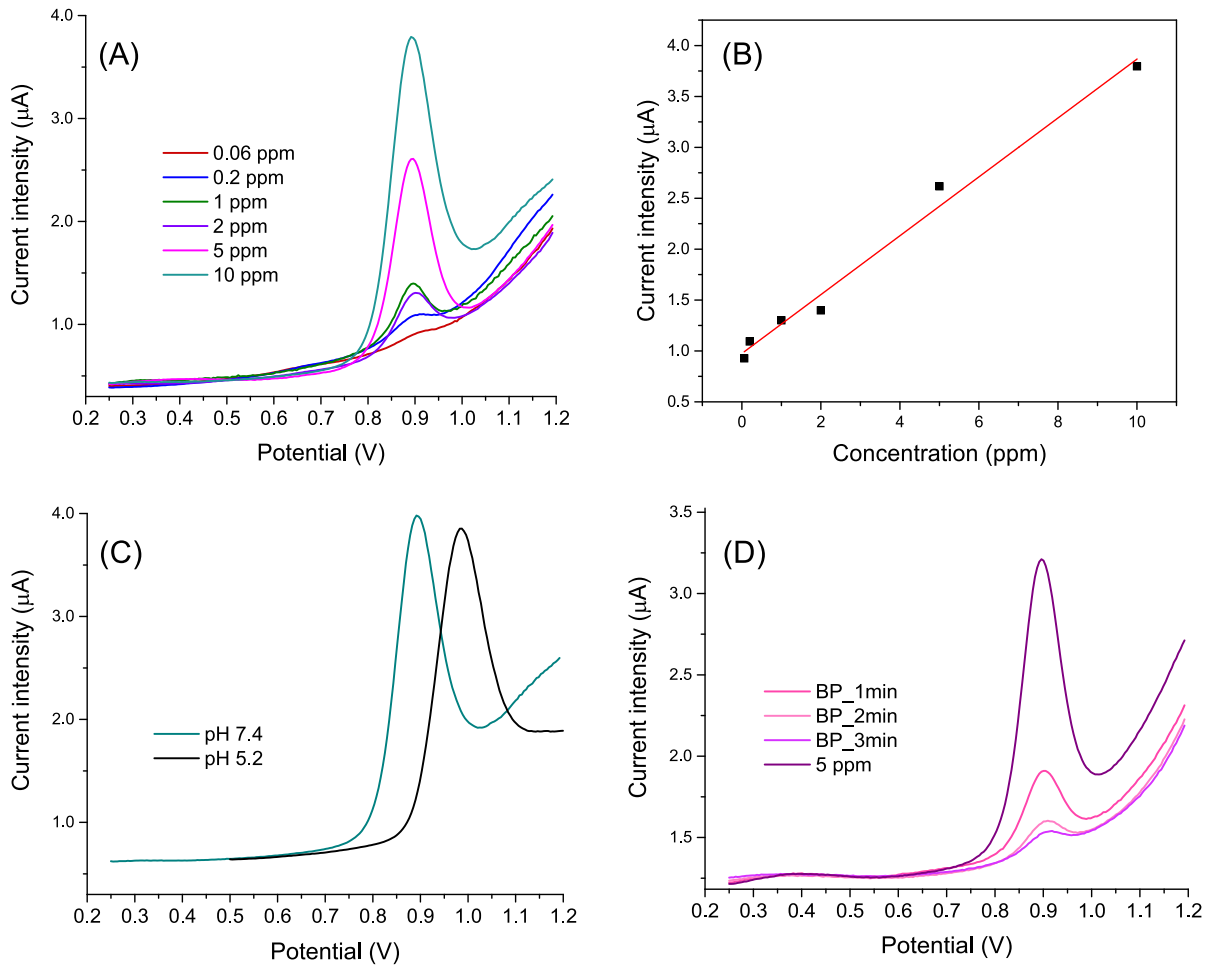

Fig. 13. (A) DPV of a CPE modified with Chol-MMSN and its response towards buffer phosphate aqueous SMX solutions in the range 0.06 to 10 ppm, (B) Calibration curve, (C) DPV of SMX 5 ppm at different pH values, and (D) desorption experiments of SMX 5 ppm in buffer phosphate, neutral pH.

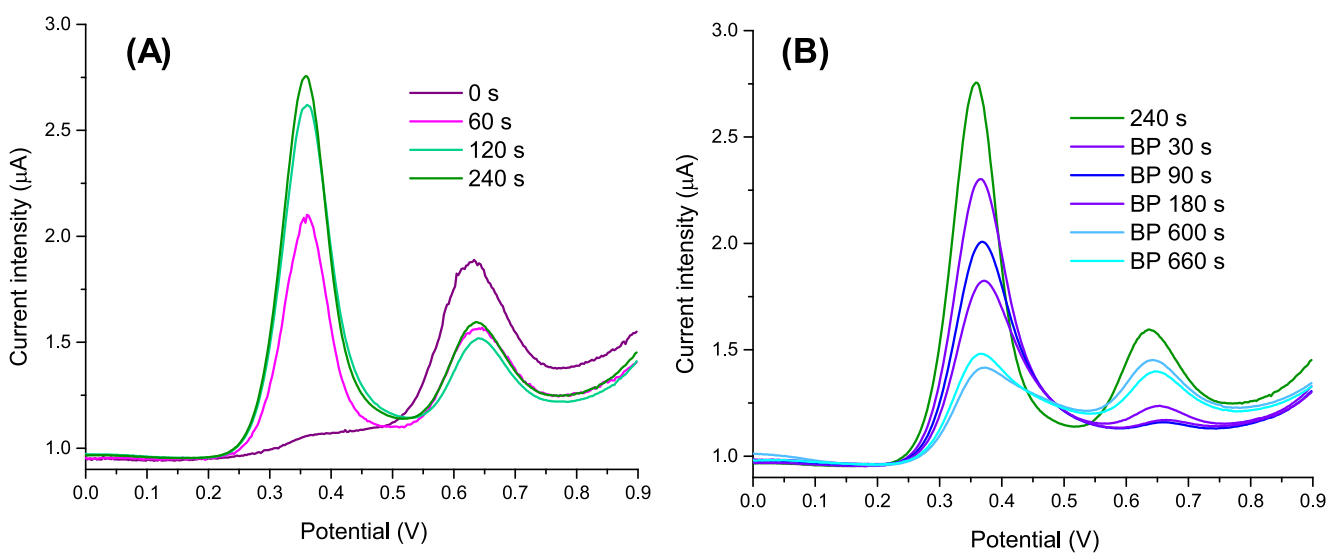

Fig. 14. (A) DPV of DF 5 ppm solution at buffer phosphate pH = 7 at different preconcentration times. (B) Desorption process measured by DPV at different times.

3.3. Adsorption isotherms and kinetic studies

The adsorption isotherms give information about the type of interaction between the adsorbate and adsorbent when the sorption process reaches equilibrium. The Langmuir, Freundlich, Sips, Temkin, and Toth isotherm empirical models were used for the DF and SMX adsorption process to examine the experimental data [28]. The parameters associated with the adsorption behaviour were calculated from the nonlinear

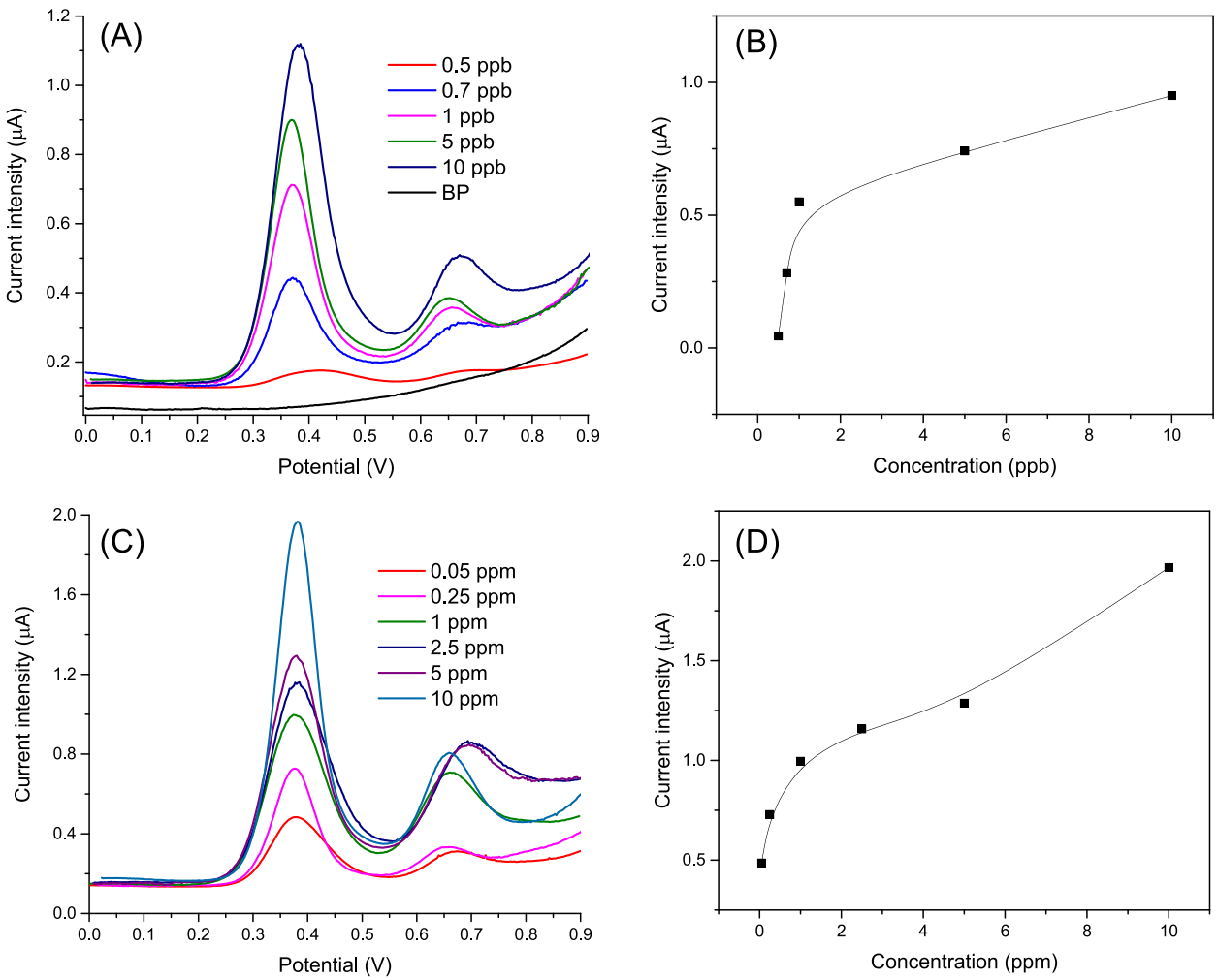

Fig. 15. DPV of a CPE modified with Chol-MMSN and its response towards buffer phosphate aqueous DF solutions in two ranges of concentration: (A) and (B) from 0.5 to 10 ppb and (C) and (D) from 0.05 to 10 ppm.

curve fit. For both drugs, the experimental adsorption data show the higher n coefficient of determination R^2 value for the Sips equation (see Table S1), an empirical model given by equation (3):

$$q_e = \frac{N_{max} K C_e^n}{1 + K C_e^n} \tag{3}$$

where N_{max} is the total number of binding sites (adsorption capacity or maximum adsorption (mg/g), K is the binding affinity constant (L^n/mg^n), and n is the heterogeneity index. Sips equation combines the Freundlich and Langmuir models. At low sorbate concentration, this equation reduces to a Freundlich isotherm while at $n = 1$ converts to the Langmuir model. The Sips isotherm describes a relationship between the concentration of bound (or active sites or adsorption at equilibrium mg/g) and free guests (Concentration at equilibrium mg/L) in both homogeneous and heterogeneous (composed of energetically different patches (or sites) surfaces. For a homogeneous material n is equal to 1 and the Sips isotherm becomes the Langmuir isotherm, describing a monolayer of adsorbate formed on the adsorbent surface. For heterogeneous materials when the exponent n is less than 1, it is rather related to a Gaussian distribution of adsorption/binding sites by energy. If K or C_e approaches 0, the Sips isotherm becomes the Freundlich isotherm. When $n > 1$, it signifies cooperative interactions, where the adsorption of one molecule enhances the adsorption of additional molecules. In some cases, the exponent may represent the formal number of molecules involved in such collaborative interaction, describing a cooperative reaction between a sorption site and n sorbate molecules, such that n is the equilibrium constant of this reaction. In this case, Equation 1 coincides with the Hill model characterizing cooperative interactions of ligand molecules with a macromolecule [29]. In the case of DF adsorption, the n value is less than 1 which indicates heterogeneous surfaces on these sorbents. Conversely, for SMX adsorption, sigmoidal type curves are obtained with n values higher than 1 for equation 1, which suggests that the adsorption process is cooperative type (Fig. 9).

The adsorption kinetics of SMX and DF were investigated to understand the adsorption mechanism. As representative samples, the adsorption capacity of Chol-MSN and PTS-Chol-MMSN, as a function of contact time for the removal of SMX and DF, were studied. It is noticeable from Fig. 10 that the adsorption capacity of both materials increased rapidly for the pollutants under study in the first 30 min and then rose slowly till the adsorption equilibrium was achieved within 6 h. To investigate the adsorption mechanism, two conventional kinetic models namely pseudo-first order and pseudo-second order were used to evaluate the experimental data as shown in Fig. 10. Overall, the pseudo-second-order equation provided good fits for both drugs (R^2 between 0.98 and 0.99), supporting the chemisorption mechanism. The pseudo-second-order model assumes that the adsorption rate is reaction-controlled. Thus, these results suggest that the adsorption rate can be governed by the electrostatic interactions between the choline and methyl p-toluene sulfonate choline functions with the anionic forms of the drugs. Similar observations have been reported regarding the kinetic profile of DF adsorption for other materials [30].

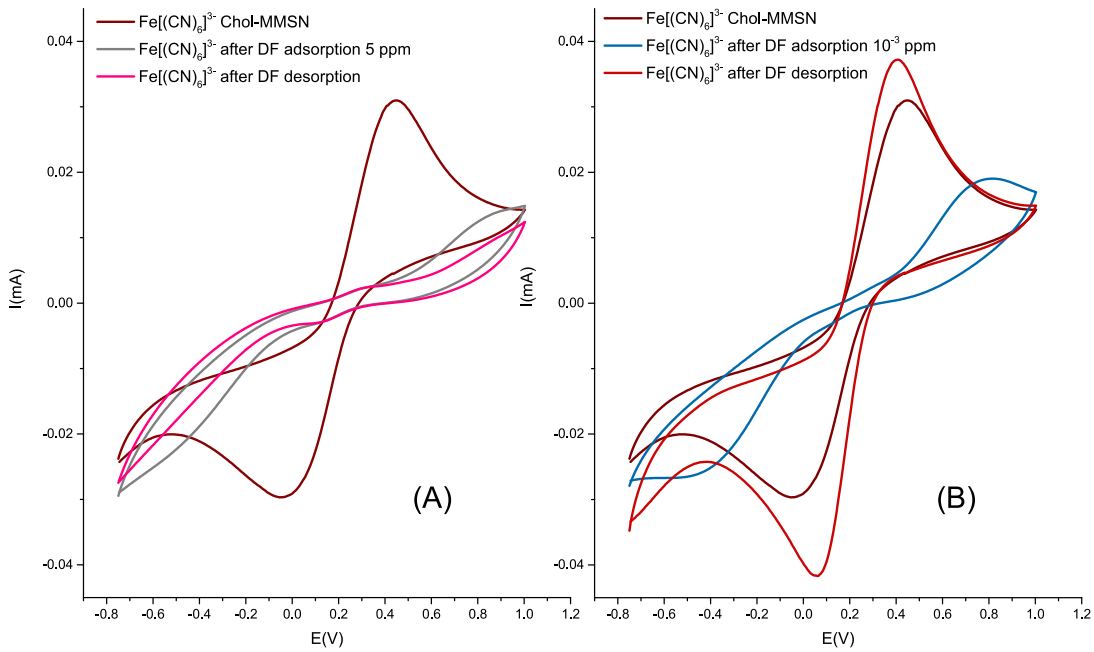

Fig. 16. Cyclic voltammetry of 5,0 mM $[Fe(CN)_6]^{3-}$ in neutral BP at scan rate 100 mV/s, and in the presence of DF 10^{-3} and 5 ppm, respectively. Scan initiated after immersion of the electrode for (A) 3 min and (B) 1 min in the DF solution.

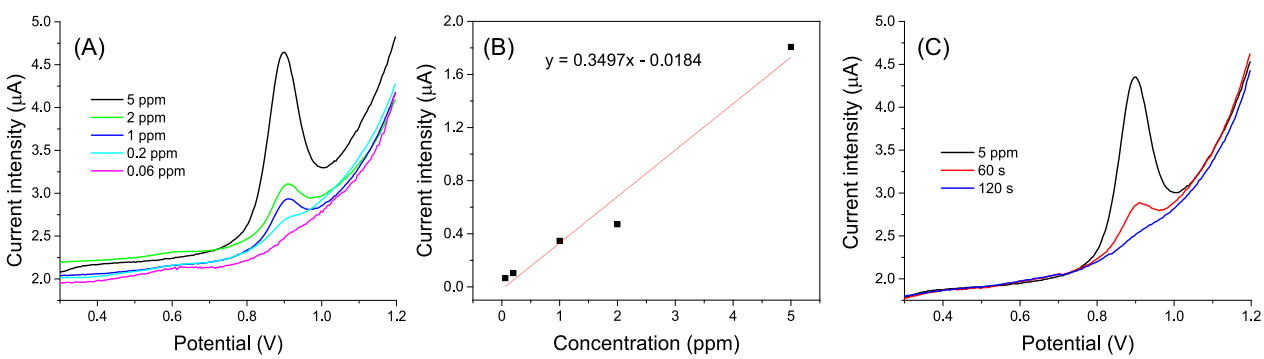

Fig. 17. (A) DPV of a CPE modified with PTS-Chol-MSN and its response towards buffer phosphate aqueous SMX solutions in the range 0.06 to 5 ppm, (B) Calibration curve, and (C) desorption experiments of SMX 5 ppm in buffer phosphate, neutral pH.

3.4. Adsorption: physical and chemical binding forces

To understand the nature of the chemical interaction established between the drugs and the most efficient adsorbents, their FTIR spectra were recorded after the adsorption procedure and compared with the FTIR of free SMX and DF drugs (Fig. 11). After SMX adsorption the most relevant features observed are the decrease of the bands attributed to the aromatic rings at 3143 cm^{-1} and the maintenance of the bands due to the amino groups. At lower wavenumbers, the bands in the range 1597–1438 cm^{-1} suffer an important reorganization which suggests the existence of additional interactions besides the electrostatic ones previously discussed, probably some type of π-π staking interactions between the aromatic rings of the SMX and the methyl p-toluene sulfonate anion on the silica surface [31]. Besides, the signal at 1266 cm^{-1} attributed to the sulfone group SO_2 decreases significantly, although in this case, it is difficult to infer additional conclusions since the other bands of this group overlap with those of silica. On the other hand, the spectrum of sodium diclofenac shows the existence of the aromatic rings in the structure which is readily determined from the C–H and C = C–C ring-related vibrations. The spectrum of free DF shows an intense, well-defined band at 1572 cm^{-1} due to ν(C = C), and additional bands from 1507 to 1397 cm^{-1} due to C–C the stretching mode of the phenyl ring and C–H in-plane bending vibrations. FTIR spectrum of adsorbed DF shows the characteristic peaks of the pure diclofenac with slight differences, for instance, the band at 1572 shifts to 1575 cm^{-1}, and the band at 1396 cm^{-1} decreases significantly and shifts to 1399 cm^{-1}. Meanwhile, the band due to the $-COO^-$ group at 1556 cm^{-1} decreases its intensity and shifts to 1557 cm^{-1}. Considering these data and the information found in the literature for this molecule [32], two types of interaction are possible: a π-π staking interaction and an electrostatic interaction through the carboxylate group and the quaternary $-N^+Me_3$ group of the choline function. Similar studies were performed with other adsorbents, but the results were not conclusive due to the low amount of drug adsorbed.

In a similar way, UV–vis spectroscopy was used to study the characteristics of the adsorbed drugs onto PTS-Chol-MSN in comparison to free drugs (Fig. 12). As can be seen, the solid-state UV–vis spectra of both drugs show strong and broad absorption bands in the range from 220 to 330 nm for DF, and from 220 to 323 for SMX. In aqueous solution, the experimental UV–vis spectra show just one intense, although broad, electronic transition at 276, and 262 nm for DF and SMX, respectively: due to strong π-π* and σ-σ* transition in the UV region with high extinction coefficients. The intensity enhancement and the narrowing of the bands in aqueous solution indicate the effect of the solvent through

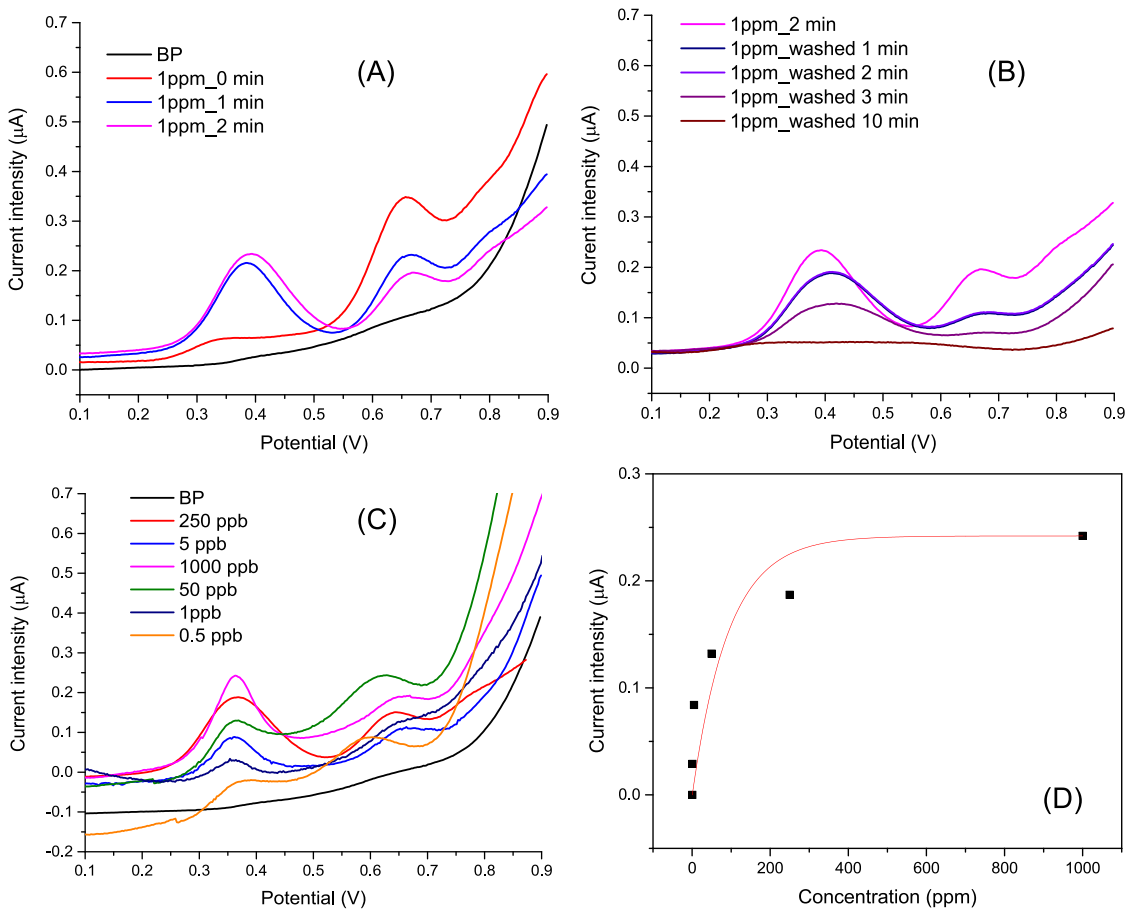

Fig. 18. A) DPV of a CPE modified with PTS-Chol-MSN and its response towards buffer phosphate aqueous DF solutions in the range 0.5 to 1000 ppb and (B) desorption experiments of DF 1 ppm in buffer phosphate, neutral pH (C) and (D) Calibration curve.

solvation and through the formation of hydrogen bonds between the drugs and the water molecules (See Figure S4). After adsorption on PTS-Chol-MSN the DR-UV–vis spectra of both drugs show much more narrow bands in accordance with the pattern observed in the aqueous solution. In comparison with the bands observed in the solution, the bands for adsorbed DF and SMX have a significant blueshift to 281 and 270 nm, respectively, which indicates that the methyl p-toluene sulfonate ring has an induction effect on the adsorbed drugs. Experimental results indicate that a combination of both physical and chemical binding forces can be involved in the DF and SMX adsorption on hybrid mesoporous silica materials. Van der Waals forces, hydrogen bonding, and electrostatic interactions play a role in the removal of these organic adsorbates [27].

As inferred from adsorption studies Chol-MMSN and Chol-MSN material shows lower adsorption performance than PTS-Chol-MMSN and PTS-Chol-MSN in terms of q_t values. However, an additional point that deserves to be studied is if these adsorbents are useful in the low concentration range in which these drugs can permeate in water treatment plants. To do so we have used these adsorbents to prepare modified carbon paste electrodes and used them as sensors in the analytical detection of the drugs under study by electrochemical techniques. As representative material the electrochemical response of carbon paste electrodes prepared with Chol-MMSN towards SMX is shown in Fig. 13. Differential pulse voltammogram (DPV) of SMX at neutral pH (Buffer phosphate electrolyte) gives a well-defined oxidation peak at 0.89 V. The current intensity of this peak due to the oxidation of the amino group on SMX establishes a linear relationship with the concentration in the range from 10 to 0.06 ppm (the detection limit was found to be 1.1 ppm). Since the adsorptive properties of PTS-Chol-MSN are being discussed, different preconcentration times were tested before performing the electrochemical measurement. It was observed that there were no differences in the measured current intensity at different preconcentration times, suggesting the rapid adsorption of the SMX molecule as indicated by the kinetic measurements.

Since pH has a significant influence on the adsorption process, a lower pH of 5.2 was also tested. This resulted in the observation of a shift in the oxidation signal to higher potentials, indicating that SMX in its anionic form is more easily oxidized. Additionally, a slight decrease in the current signal was noted. Considering that most of the reported data are measured at neutral pH, these observations prompted us to conduct the measurements at neutral pH moving forward. When the electrode was immersed in a phosphate buffer solution, consecutive measurements were recorded, and it was observed that the signal attributed to SMX decreased significantly, suggesting that the desorption process occurred in less than 3 min.

Similarly, the voltametric detection of DF was studied using Chol-MMSN to modify carbon paste electrodes. Traditionally, the detection of DF relies on analyzing the anodic peak corresponding to the direct oxidation of DF, which occurs at around 0.56 V due to its pK_a value of 4.15. However, the electrochemical oxidation of diclofenac follows an EC mechanism, where the electrochemical reaction involves the exchange of one electron, while the chemical reaction involves the breakdown of the oxidation product through the nitrogen atom, resulting in the formation of 2,6-dichloroaniline and 2-(2-hydroxyphenyl) acetic acid. During the second sweep, one new anodic peak appears at 0.333 V, this could be related to the oxidation of 1-hydroxy-2-(hydroxyphenyl) ethanalate (previously formed) to 2-(2-hydroxyphenyl) acetic acid. This decomposition reaction was exploited by Cid-

Cerón and co-workers [33] to propose a new methodology for quantifying DF, focusing on the peak corresponding to 1-hydroxy-2-(hydroxyphenyl) ethanalate. Similarly, we have adopted this approach in our experiments. Initially, we investigated the effect of preconcentration time as a variable in the adsorption process of DF on the surface of the carbon paste electrode modified with Chol-MMSN.

As shown in Fig. 14, the first scan labeled as "0 s" time displays a peak at 0.63 V, which is attributed to the oxidation of adsorbed DF. Subsequent scans revealed a linear increase in the current intensity of a new peak at 0.36 V, corresponding to 1-hydroxy-2-(hydroxyphenyl) ethanalate, the decomposition product of DF. The current intensity reaches saturation after 4 min of preconcentration time.

When the electrode is immersed in a pure phosphate buffer solution and consecutive measurements are performed, the signal attributed to 1-hydroxy-2-(hydroxyphenyl) ethanalate decreases significantly. However, in this case, the desorption process requires more than 10 min to reach the lower value, and it is not complete. This is evident from the presence of two anodic peaks at 0.63 V and 0.36 V, respectively, indicating the incomplete desorption of both 1-hydroxy-2-(hydroxyphenyl) ethanalate and DF itself. These findings support the higher affinity of Chol-MMSN towards DF compared to SMX, as previously observed in batch experiments.

The higher affinity of the Chol-MMSN adsorbent towards DF is also evident in the relationship discovered between the concentration and the current intensity of the peak at 0.36 V. Fig. 15A and B depict two different concentration ranges: 0.5–10 ppb with preconcentration times of 3 min and 0.05–10 ppm with preconcentration times of 1 min (prior to measurements). In both calibration curves, the limit of linearity is established at low concentrations, indicating that the electrode is highly sensitive to concentrations below 1 μg/L. It is evident that this material has the potential to be used for the development of a sensitive electrochemical sensor for DF analysis, provided that an appropriate preconcentration time is employed. However, this aspect falls beyond the scope of this study.

Cyclic voltammetry (CV) of the electroactive $[Fe(CN)_6]^{3-}$ has been employed to assess the potential recovery and subsequent recycling of the adsorbents. The extent of kinetic hindrance in the electron transfer process of $[Fe(CN)_6]^{3-}$ as a molecular probe increases with greater thickness and reduced defect density of the barrier. In other words, a higher adsorption of the drug by the surface electrode is expected to result in lower redox transfer kinetics for the molecular probe. Fig. 16A and B illustrate the CV responses of 5 mM $[Fe(CN)_6]^{3-/4-}$ in phosphate buffer solution (pH 7.4) at a bare modified carbon paste electrode (MCPE) with Chol-MMSN, both before and after DF adsorption, respectively. At the bare MCPE, $[Fe(CN)_6]^{3-/4-}$ generates well-defined redox waves with a peak-to-peak separation of 496 mV using a scan rate of 100 mV/s.

The linear relationship between current intensity and the square root of the scan speed confirms the diffusional behavior of the electroactive molecule, as shown in Figure S5. When the electrode is immersed in a DF solution and the drug adsorbs onto the modified Chol-MMSN support, a noticeable decrease in the redox peak current associated with the probe molecule is observed. This indicates that DF, when adsorbed on the hybrid silica surface, acts as a mass transfer blocking layer, impeding the diffusion of ferricyanide towards the electrode surface.

The CV of the same MCPE electrode, thoroughly washed with water and immersed in a phosphate buffer, reveals that the peak current is essentially recovered when a more diluted solution of DF (10^{-3} ppm) is used. This suggests that the drug can be efficiently desorbed from the silica surface. However, when a more concentrated solution (5 ppm) is used to form an MCPE-coated film with the drug, the washing procedure is unable to completely remove the adsorbed drug from the silica surface. Consequently, the electrode remains saturated, and the peak current remains unaltered, supporting the stability of the coated electrode and the efficient adsorption process of diclofenac.

These findings were further validated through a batch experiment involving the recycling of Chol-MMSN used to adsorb the 50-ppm stock DF solution used to generate the data in Table 1. The results showed that the material experiences a 22 % decrease in efficiency during the first run, indicating some loss in its adsorption capacity.

To study the influence of methyl p-toluene sulfonate choline as functionality on silica surface, PTS-Chol-MSN was chosen as representative material (Fig. 17). DPV of SMX at neutral pH (Buffer phosphate electrolyte) revealed without a preconcentration time a well-defined oxidation peak at 0.89 V, similar to potential observed with choline functionality on Chol-MMSN. Equally, this peak exhibited a linear relationship with the concentration ranging from 5 to 0.06 ppm. The detection limit was determined to be 1.2 ppm, slightly higher than that found for Chol-MMSN. To gather information about the desorption process, the modified electrode was immersed in a buffer phosphate solution, and new consecutive measurements were recorded, the signal attributed to SMX significantly decreased, indicating that the desorption process occurs in less than 2 min.

The CV of electroactive $[Fe(CN)_6]^{3-}$ in BP pH 7,4 at a MCP electrode modified with PTS-Chol-MSN produces an ill-defined redox wave with a very high peak-to-peak separation of approximately 900 mV at a scan rate of 100 mV/s (See Figure S6). This outcome indicates that the methyl p-toluene sulfonate counterion introduces an important kinetic hindrance to the electron transfer between the molecular probe and the electrode rendering this material unsuitable for further CV analysis after adsorption.

The adsorption process of DF on the surface of the PTS-Chol-MSN modified carbon paste electrode was also studied. As can be seen, in Fig. 18, the first scan labelled as 0 s time shows a peak at 0.63 V attributed to the oxidation of adsorbed DF, successive scans shows that a linear increase in the preconcentration time is highly related to the current intensity of the peak at 0.36 V due to 1-hydroxy-2-(hydroxyphenyl) ethanalate. Current intensity peak reaches saturation after 2 min of preconcentration time. When the electrode is immersed in a pure buffer phosphate solution and new consecutive measurements are performed, the signal attributed to 1-hydroxy-2-(hydroxyphenyl) ethanalate decreases significantly, but in this case the desorption needs more than 10 min to reach the lower value and it is not complete, neither the desorption of DF itself, as can be seen by observing the presence of two anodic peaks at 0.63 and 0.36 V, respectively. This behaviour supports the higher affinity of PTS-Chol-MSN towards DF in comparison to SMX, as previously observed in batch experiments. Similarly, to Chol-MMSN behaviour, the calibration curve of PTS-Chol-MSN towards DF shows that the limit of linearity is established at low concentrations, which indicates that the electrode is highly sensitive towards concentrations below 1 μg/L.

4. Conclusions

In this study, the potential of hybrid core–shell magnetic mesoporous silica nanospheres and mesoporous silica nanospheres as adsorbents for the removal of diclofenac and sulfomethoxazole has been investigated. The research focuses on exploring various variables, including surface physical properties and chemical surface properties, to design efficient mesoporous silica adsorbents for organic drugs such as DF and SMX.

The findings indicate that materials with higher surface area, such as MSN, are preferred in comparison to MMSN. The chemical surface properties can be customized by changing the nature of the functionality on the silica surface and controlling the surface density of silanol groups. The presence of specific adsorbent sites on the silica, such as sulfonate groups capable of establishing π-π interactions, plays an important role in the mechanism process.

Moreover, the presence of silanol groups on the silica surface not only influences the material's surface charge and the establishment of electrostatic interactions but also facilitates the formation of chemical interactions via hydrogen bond formation. This has been demonstrated by comparing the materials with their silylated counterparts.

The synergic effect of the different factors renders the material PTS-Chol-MSN an efficient adsorbent capable of removing 94 % and 50 % of DF and SMX from water in batch experiments. The varying adsorption efficiency values showed by the hybrid mesoporous silica materials at different drug concentrations suggest their suitability for incorporation into conventional membranes or carbonaceous supports to be used as preconcentrating devices or sensors.

CRediT authorship contribution statement

Josefa Ortiz-Bustos: Conceptualization, Data curation, Investigation, Writing – review & editing. **Sofia F. Soares:** Investigation. **Helena Pérez del Pulgar:** Investigation. **Yolanda Pérez:** Investigation. **Santiago Gómez-Ruiz:** Funding acquisition, Writing – review & editing. **Ana Luísa Daniel-da-Silva:** Funding acquisition, Investigation, Writing – review & editing. **Isabel del Hierro:** Conceptualization, Data curation, Funding acquisition, Investigation, Writing – original draft.

Declaration of competing interest

The authors declare that they have no known competing financial interests or personal relationships that could have appeared to influence the work reported in this paper.

Data availability

No data was used for the research described in the article.

Acknowledgements

We would like to thank funding from the research project PID2022-136417NB-I00 financed by MCIN/AEI/10.13039/501100011033/ and "ERDF A way of making Europe". and Salvador de Madariaga Program (scholarship PRX18/00290 for Dr. I del Hierro) (Spain), and the projects CICECO-Aveiro Institute of Materials, UIDB/50011/2020, UIDP/50011/2020 and LA/P/0006/2020, financed by national funds through the FCT/MCTES (PIDDAC) (Portugal).

Appendix A. Supplementary material

Supplementary data to this article can be found online at https://doi.org/10.1016/j.molliq.2024.124213.

References

[1] M. Gavrilescu, K. Demnerová, J. Aamand, S. Agathos, F. Fava, Emerging pollutants in the environment: present and future challenges in biomonitoring, ecological risks and bioremediation, N. Biotechnol. 32 (2015) 147–156, https://doi.org/10.1016/j.nbt.2014.01.001.
[2] Z. Cheng, H. Dong, J. Liang, F. Zhang, X. Chen, L. Du, K. Tan, Highly selective fluorescent visual detection of perfluorooctane sulfonate via blue fluorescent carbon dots and berberine chloride hydrate, Spectrochim. Acta A Mol. Biomol. Spectrosc. 207 (2019) 262–269, https://doi.org/10.1016/j.saa.2018.09.028.
[3] H. Ryu, B. Li, S. De Guise, J. McCutcheon, Y. Lei, Recent progress in the detection of emerging contaminants PFASs, J. Hazard. Mater. 408 (2021) 124437, https://doi.org/10.1016/j.jhazmat.2020.124437.
[4] C. Teodosiu, A. Gilca, G. Barjoveanu, S. Fiore, Emerging pollutants removal through advanced drinking water treatment: A review on processes and environmental performances assessment, J. Clean. Prod. 197 (2018) 1210–1221, https://doi.org/10.1016/j.jclepro.2018.06.247.
[5] Y. Patiño, E. Díaz, S. Ordóñez, Performance of different carbonaceous materials for emerging pollutants adsorption, Chemosphere 119 (2015) S124–S130, https://doi.org/10.1016/j.chemosphere.2014.05.025.
[6] V. Calisto, C.I.A. Ferreira, J.A.B.P. Oliveira, M. Otero, V.I. Esteves, Adsorptive removal of pharmaceuticals from water by commercial and waste-based carbons, J. Environ. Manage. 152 (2015) 83–90, https://doi.org/10.1016/j.jenvman.2015.01.019.
[7] A.O. Abo El Naga, M. El Saied, S.A. Shaban, F.Y. El Kady, Fast removal of diclofenac sodium from aqueous solution using sugar cane bagasse-derived activated carbon, J. Mol. Liq. 285 (2019) 9–19, https://doi.org/10.1016/j.molliq.2019.04.062.
[8] A. Gil, L. Santamaría, S.A. Korili, M.A. Vicente, L.V. Barbosa, S.D. de Souza, L. Marçal, E.H. de Faria, K.J. Ciuffi, A review of organic-inorganic hybrid clay based adsorbents for contaminants removal: Synthesis, perspectives and applications, J. Environ. Chem. Eng. 9 (2021) 105808, https://doi.org/10.1016/j.jece.2021.105808.
[9] M. Khraisheh, S. Elhenawy, F. AlMomani, M. Al-Ghouti, M.K. Hassan, B. H. Hameed, Recent Progress on Nanomaterial-Based Membranes for Water Treatment, Membranes 11 (2021), https://doi.org/10.3390/membranes11120995.
[10] B. Czech, P. Oleszczuk, Sorption of diclofenac and naproxen onto MWCNT in model wastewater treated by H2O2 and/or UV, Chemosphere 149 (2016) 272–278, https://doi.org/10.1016/j.chemosphere.2015.12.057.
[11] A.C. Estrada, A.L. Daniel-da-Silva, C. Leal, C. Monteiro, C.B. Lopes, H.I.S. Nogueira, I. Lopes, M.J. Martins, N.C.T. Martins, N.P.F. Gonçalves, S. Fateixa, T. Trindade, Colloidal nanomaterials for water quality improvement and monitoring, Front. Chem. 10 (2022).
[12] M. Fischer, Simulation-based evaluation of zeolite adsorbents for the removal of emerging contaminants, Materials Advances. 1 (2020) 86–98, https://doi.org/10.1039/d0ma00025f.
[13] S. Singh, R. Garg, A. Jana, C. Bathula, S. Naik, M. Mittal, Current developments in nanostructurally engineered metal oxide for removal of contaminants in water, Ceram. Int. 49 (2023) 7308–7321, https://doi.org/10.1016/j.ceramint.2022.10.183.
[14] E. Kowalska, M. Endo, Z. Wei, K. Wang, M. Janczarek, Chapter 21 - Noble Metal Nanoparticles for Water Purification, in: S. Thomas, D. Pasquini, S. Leu, D. A. Gopakumar (Eds.), Nanoscale Materials in Water Purification, Elsevier, 2019, pp. 553–579.
[15] B. Sarkar, S. Mandal, Y.F. Tsang, P. Kumar, K. Kim, Y.S. Ok, Designer carbon nanotubes for contaminant removal in water and wastewater: A critical review, Sci. Total Environ. 612 (2018) 561–581, https://doi.org/10.1016/j.scitotenv.2017.08.132.
[16] A.M.E. Khalil, F.A. Memon, T.A. Tabish, D. Salmon, S. Zhang, D. Butler, Nanostructured porous graphene for efficient removal of emerging contaminants (pharmaceuticals) from water, Chem. Eng. J. 398 (2020) 125440, https://doi.org/10.1016/j.cej.2020.125440.
[17] V.B. Cashin, D.S. Eldridge, A. Yu, D. Zhao, Surface functionalization and manipulation of mesoporous silica adsorbents for improved removal of pollutants: a review, Environ. Sci. : Water Res. Technol. 4 (2018) 110–128, https://doi.org/10.1039/C7EW00322F.
[18] S.A. Jadhav, V.S. Patil, P.S. Shinde, S.S. Thoravat, P.S. Patil, A short review on recent progress in mesoporous silicas for the removal of metal ions from water, Chem. Pap. 74 (2020) 4143–4157, https://doi.org/10.1007/s11696-020-01255-6.
[19] R. Goutham, P. Rohit, S.S. Vigneshwar, A. Swetha, J. Arun, K.P. Gopinath, A. Pugazhendhi, Ionic liquids in wastewater treatment: A review on pollutant removal and degradation, recovery of ionic liquids, economics and future perspectives, J. Mol. Liq. 349 (2022) 118150, https://doi.org/10.1016/j.molliq.2021.118150.
[20] P. Isosaari, V. Srivastava, M. Sillanpää, Ionic liquid-based water treatment technologies for organic pollutants: Current status and future prospects of ionic liquid mediated technologies, Sci. Total Environ. 690 (2019) 604–619, https://doi.org/10.1016/j.scitotenv.2019.06.421.
[21] K. Friess, P. Izák, M. Kárászová, M. Pasichnyk, M. Lanč, D. Nikolaeva, P. Luis, J. C. Jansen, A Review on Ionic Liquid Gas Separation Membranes, Membranes (basel). 11 (2021) 97, https://doi.org/10.3390/membranes11020097.
[22] B.L. Gadilohar, G.S. Shankarling, Choline based ionic liquids and their applications in organic transformation, J. Mol. Liq. 227 (2017) 234–261, https://doi.org/10.1016/j.molliq.2016.11.136.
[23] P. Cruz, Y. Pérez, I. del Hierro, Titanium alkoxides immobilized on magnetic mesoporous silica nanoparticles and their characterization by solid state voltammetry techniques: Application in ring opening polymerization, Microporous Mesoporous Mater. 240 (2017) 227–235, https://doi.org/10.1016/j.micromeso.2016.11.028.
[24] J. Ortiz-Bustos, Y. Pérez, I. del Hierro, Structure, stability, electrochemical and catalytic properties of polyoxometalates immobilized on choline-based hybrid mesoporous silica, Microporous Mesoporous Mater. 321 (2021) 111128, https://doi.org/10.1016/j.micromeso.2021.111128.
[25] D. Archundia, C. Duwig, L. Spadini, M.C. Morel, B. Prado, M.P. Perez, V. Orsag, J. M.F. Martins, Assessment of the Sulfamethoxazole mobility in natural soils and of the risk of contamination of water resources at the catchment scale, Environ. Int. 130 (2019) 104905, https://doi.org/10.1016/j.envint.2019.104905.
[26] D. Singappuli-Arachchige, I.I. Slowing, Control of interfacial pH in mesoporous silica nanoparticles via surface functionalization, J. Chem. Phys. 152 (2020) 034703, https://doi.org/10.1063/1.5138912.
[27] M.S. Shamsudin, S.F. Azha, L. Sellaoui, M. Badawi, A. Bonilla-Petriciolet, S. Ismail, Performance and interactions of diclofenac adsorption using Alginate/Carbon-based Films: Experimental investigation and statistical physics modelling, Chem. Eng. J. 428 (2022) 131929, https://doi.org/10.1016/j.cej.2021.131929.

[28] J. Wang, X. Guo, Adsorption isotherm models: Classification, physical meaning, application and solving method, Chemosphere 258 (2020) 127279, https://doi.org/10.1016/j.chemosphere.2020.127279.
[29] Y. Keren, M. Borisover, N. Bukhanovsky, Sorption interactions of organic compounds with soils affected by agricultural olive mill wastewater, Chemosphere 138 (2015) 462–468, https://doi.org/10.1016/j.chemosphere.2015.06.085.
[30] S.F. Soares, T. Trindade, A.L. Daniel-da-Silva, Enhanced removal of non-steroidal inflammatory drugs from water by quaternary chitosan-based magnetic nanosorbents, Coatings 11 (2021), https://doi.org/10.3390/coatings11080964.
[31] K. Szabó, P. Wang, B. Peles-Lemli, Y. Fang, L. Kollár, S. Kunsági-Máté, Structure of aggregate of hydrotropic p-toluene sulfonate and hydroxyacetophenone isomers, Colloids Surf. Physicochem. Eng. Aspects. 422 (2013) 143–147, https://doi.org/10.1016/j.colsurfa.2013.01.034.
[32] I.M. Kenawi, B.N. Barsoum, M.A. Youssef, Drug–drug interaction between diclofenac, cetirizine and ranitidine, J. Pharm. Biomed. Anal. 37 (2005) 655–661, https://doi.org/10.1016/j.jpba.2004.10.051.
[33] M.M. Cid-Cerón, D.S. Guzmán-Hernández, M.T. Ramírez-Silva, A. Galano, M. Romero-Romo, M. Palomar-Pardavé, New insigths on the kinetics and mechanism of the electrochemical oxidation of diclofenac in neutral aqueous medium, Electrochim. Acta. 199 (2016) 92–98, https://doi.org/10.1016/j.electacta.2016.03.094.
[34] A. Adam, K. Parkhomenko, P. Duenas-Ramirez, C. Nadal, G. Cotin, P. Zorn, P. Choquet, S. Bégin-Colin, D. Mertz, Orienting the pore morphology of core-shell magnetic mesoporous silica with the sol-gel temperature. influence on MRI and magnetic hyperthermia properties, Molecules 26 (2021), https://doi.org/10.3390/molecules26040971.